Faults (shear zones) in the Earth's mantle

Alain Vauchez, Andrea Tommasi, David Mainprice

Faults (shear zones) in the Earth's mantle

Alain Vauchez *, Andréa Tommasi, David Mainprice

Geosciences Montpellier, CNRS & Univ. Montpellier 2, Univ. Montpellier 2, cc. 60, Pl. E. Bataillon, F-34095 Montpellier cedex5, France

Geodetic data support a short-term continental deformation localized in faults bounding lithospheric blocks. Whether major "faults" observed at the surface affect the lithospheric mantle and, if so, how strain is distributed are major issues for understanding the mechanical behavior of lithospheric plates. A variety of evidence, from direct observations of deformed peridotites in orogenic massifs, ophiolites, and mantle xenoliths to seismic reflectors and seismic anisotropy beneath major fault zones, consistently supports prolongation of major faults into the lithospheric mantle. This review highlights that many aspects of the lithospheric mantle deformation remain however poorly understood. Coupling between deformation in frictional faults in the uppermost crust and localized shearing in the ductile crust and mantle is required to explain the post-seismic deformation, but mantle viscosities deduced from geodetic data and extrapolated from laboratory experiments are only reconciled if temperatures in the shallow lithospheric mantle are high (>800 °C at the Moho). Seismic anisotropy, especially shear wave splitting, provides strong evidence for coherent deformation over domains several tens of km wide in the lithospheric mantle beneath major transcurrent faults. Yet it cannot detect narrow strain localization zones or shallowly dipping faults. Seismic profiling images shallow-dipping seismic reflectors in the lithospheric mantle interpreted as the continuation of normal or, less frequently, inverse faults in the mantle. However the nature of these reflectors is poorly understood. There is a large discrepancy between the scale at which deformation processes are studied (a few kilometers, at most, due to the limited size of continuous mantle exposures at the Earth's surface) and the scale inferred for strain localization in the mantle from geophysical observations (tens of kilometers). Combining data on deformation microstructures and crystal preferred orientations in naturally deformed peridotites and seismologic observations allows nevertheless discussing strain localization processes that may play a role on the development of mantle shear zones.

* Corresponding author. Tel.: 33 467 14 38 95; fax: 33 467 14 36 03.
E-mail addresses: alain.vauchez@um2.fr (A. Vauchez), andrea.tommasi@gm.univ-montp2.fr (A. Tommasi), david@gm.univ-montp2.fr (D. Mainprice).

1. Introduction

Faults are discontinuities accommodating differential motions between relatively undeformed blocks at the Earth's surface. GPS measurements in Anatolia (Hollenstein et al., 2008; McClusky et al., 2000; Reilinger et al., 2006), Asia (Zhang et al., 2004), and western North America (Argus and Gordon, 2001; d'Alessio et al., 2005) show that velocity vectors are consistent over large continental domains, but differ drastically between blocks (Fig. 1). Observed velocity gradients are usually consistent with the slip directions and rates estimated in block-bounding faults. Such observations led Reilinger et al. (2006) and Thatcher (2007) to propose that the velocity fields in the Arabia–Africa–Eurasia plate boundary (Fig. 1B) and in Asia (Fig. 2) may be explained by a model of rigid blocks in which motion is accommodated by slip along faults at the block boundaries and hence that most continental deformation is localized in fault zones rather than distributed. The size of these "undeformed" blocks and the magnitude of the relative displacement of neighboring blocks are large enough to suggest that the entire lithosphere is involved in the deformation.

More than 40 years of structural geology and geophysics have shown that faults are complex structures (*cf.* review in Handy et al., 2007). They penetrate deep into the crust and, when crossing the brittle–ductile transition, are no longer characterized by a discontinuity, but by a localized zone of continuous deformation dominated by simple shear, in which the differential displacement between two blocks is accommodated. They become "shear zones". A more general definition of a fault (the one we will use here) is therefore a zone of more or less intense strain localization accommodating a velocity gradient between two lithospheric domains. Temperature, pressure, strain rate, stress, mineralogy, rock microstructure, and water content determine which deformation mechanisms will accommodate the velocity gradient across the fault at a given depth (*e.g.*, Handy, 1989). Adaptation to the local physical conditions involves changes in dominant deformation mechanism, as the transition from brittle failure to cataclastic flow in the brittle upper crust (Fig. 3). In the ductile regime, it results in variations in the dominant slip systems in minerals deforming by dislocation creep, such as quartz or calcite, or in transition between grain-size insensitive and grain-size sensitive creep.

Variation in physico-chemical conditions with depth results therefore in changes in the degree of strain localization (and hence in the thickness of a shear zone; Figs. 3 and 4). Strain localization is extreme (thin shear zones) in the uppermost crust, where brittle behavior dominates, and moderate (wide shear zones) in the middle to lower crust (Leloup et al., 1995; Platt and Behr, 2011; Sibson, 1977; Vauchez and Tommasi, 2003; Vauchez et al., 2005). Shear zones several tens of kilometers wide in the middle to lower crust have been described in several orogens (Fig. 5; *cf.* reviews in Storti et al., 2003; Vauchez and Tommasi, 2003 and references herein). Strain is distributed over still wider domains (100 km-scale) in the middle to lower crust of hot orogens characterized by high thermal gradients and slow cooling rates (>35 °C/km and <5 °C/My; *e.g.*, Goscombe and Gray, 2008; Vauchez et al., 2007). These observations

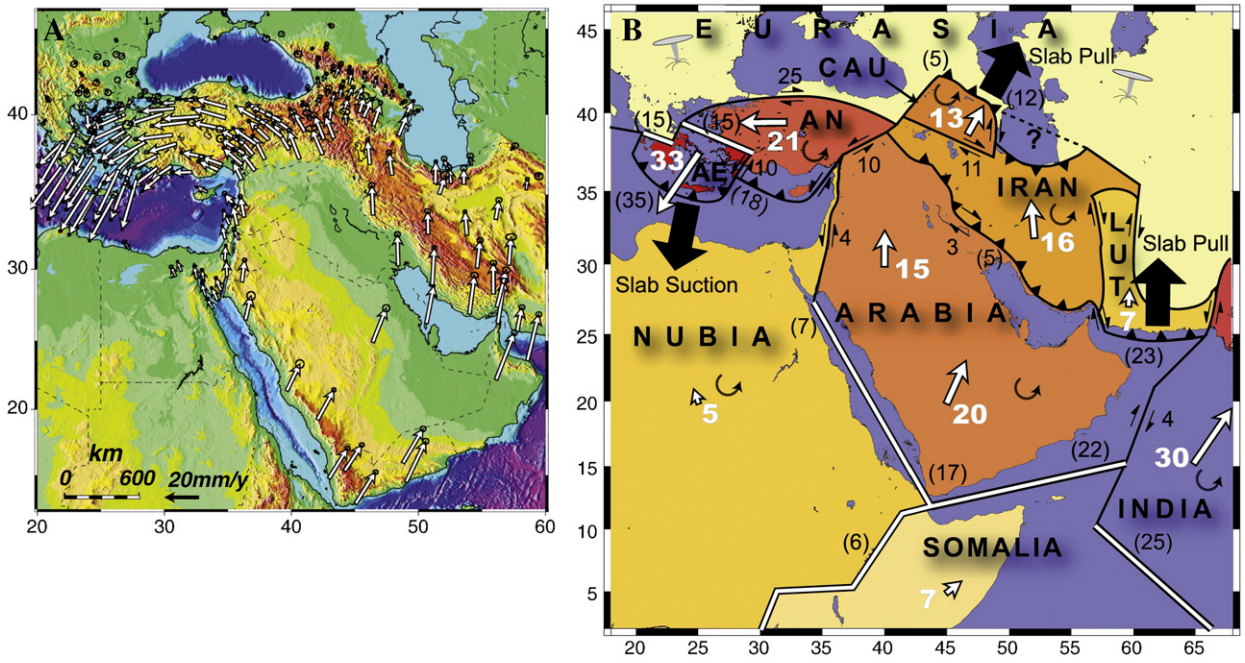

Fig. 1. Active deformation in the eastern Mediterranean domain. (A) GPS velocity vectors relative to Eurasia with 1σ uncertainties (Reilinger et al., 2006) showing the lateral escape of Anatolia due to Arabia–Europa convergence. (B) Schematic map showing the lithospheric blocks in the Arabia–Africa–Eurasia zone and the block boundaries in which most of the active deformation is accommodated (Reilinger et al., 2006). White arrows are velocity vectors relative to Eurasia determined from GPS measurements, white number is block velocity in mm/y. The tectonic blocks are bounded by active faults in which the differential displacement between blocks is accommodated by lithospheric deformation. Convergent boundaries are marked by triangles and strike-slip by double arrows. Double lines show extensional boundaries (rifts or oceanic ridges). Curved arrows illustrate block rotation. Dark numbers are slip rates (mm/y) on block-bounding faults derived from GPS velocities. Large dark arrows are hypothesized tectonic forces. CAU = Caucasus; AN = Anatolia; AE = Aegean plate.

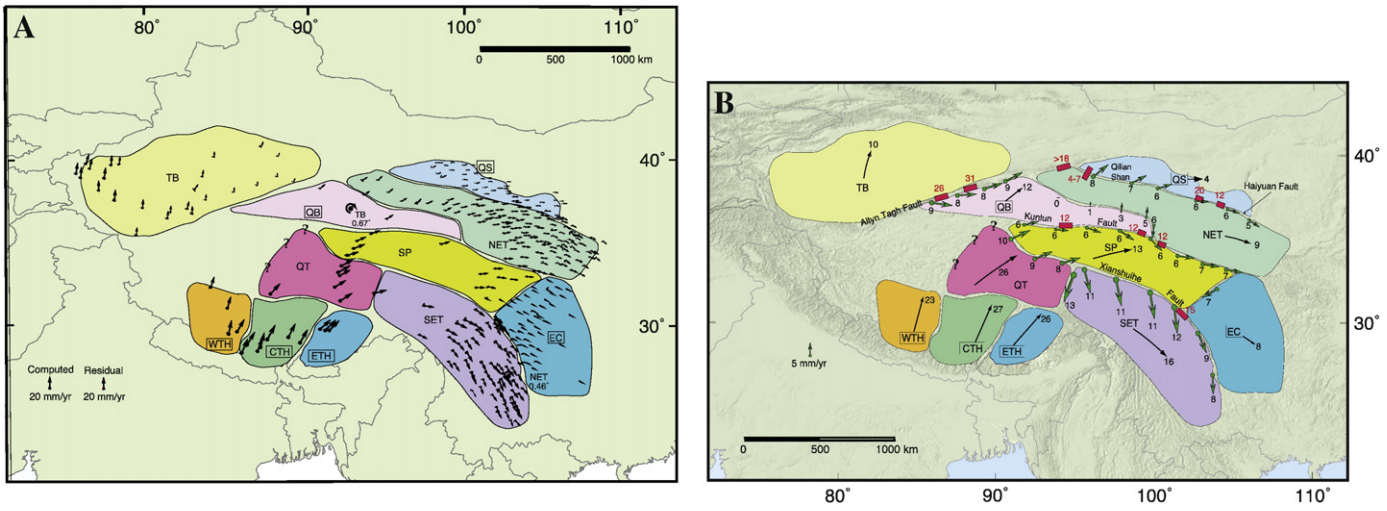

Fig. 2. Velocity vectors (black arrows), lithospheric blocks and strain localization in block-bounding faults in Tibet (Thatcher, 2007). (A) Velocity field relative to Eurasia computed from GPS measurement and lithospheric blocks deduced from those measurements. Small arrows (frequently too small to be visible) are differences between observed and computed velocities. (B) Average velocity (black arrow) for each block, predicted interblock velocities (thicker green arrows) and slip rate for block-bounding faults deduced from geological observations (red numbers and associated thick red line for locating the fault segment on which slip rate determination was made). (CTH, central Tibet Himalaya; EC, east China; ETH, eastern Tibet Himalaya; NET, northeast Tibet; QB, Qaidam Basin; QS, Qilian Shan; QT, Qiangtang; SET, southeast Tibet; SP, Songpan; TB, Tarim Basin; WTH, western Tibet Himalaya).

point to a complex and subtle balance between deformation processes and strain localization allowing faults to accommodate large-scale velocity gradients at different depths in the crust. Does the lithospheric mantle behave in the same way? Is deformation localized or distributed? The answer depends both on the scale of observation and on the scale of the analyzed system. "Strain localization" may be defined as the accommodation of significant strain gradients on a scale significantly smaller than the local or the bulk tectonic system. A "system-based" definition may result in very wide strain localization zones. For instance, shear zones 30–40 km wide in the middle/lower crust of an orogenic belt several hundreds to ~1000 km wide do represent strain localization since they are characterized by an organized flow fabric that strongly contrasts with the regional strain field outside the shear zones.

A strong argument in favor of faults affecting the lithospheric mantle comes from geodetic monitoring of active faults. Analysis of synthetic aperture radar (InSAR) and GPS data collected after the Landers and Hector Mine earthquakes revealed that these events were followed by a long period (months to years) during which strain rate was significantly higher than the average inter-seismic strain rate (Pollitz et al., 2000). These observations were successfully explained by a model of post-seismic deformation controlled by viscoelastic relaxation in the lower crust and upper mantle beneath the active faults (Pollitz et al., 2001). The same process was proposed as a likely explanation for post-seismic deformation following the M7.9 2002 Denali earthquake in Alaska (Pollitz, 2005) and the June 2000 South Iceland earthquake sequence (Árnadóttir et al., 2005), and for the present-day deformation in the Central Nevada Seismic Belt

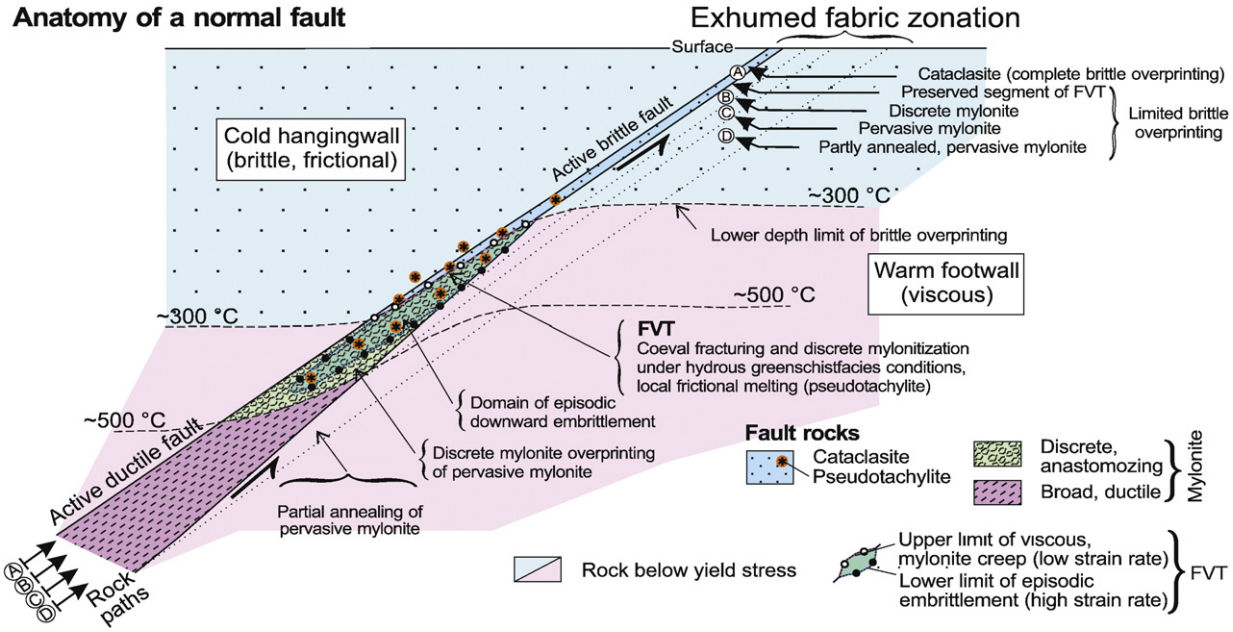

Fig. 3. Anatomy of a normal fault from Handy et al. (2007). This figure illustrates the changes in mechanical behavior/deformation mechanism and microstructure/fault rock type within a crustal scale normal fault. Besides the variations due to the initial thermal gradient within the crust, the progressive exhumation of the footwall involves cooling of the rocks, changes in deformation mechanisms and further strain localization, resulting in a fabric zonation. This evolution is also valid for the lithospheric mantle as supported by zonation observed in normal faults in peridotite massifs (e.g. Kaczmarek and Tommasi, 2011). FVT is for frictional-to-viscous transition.

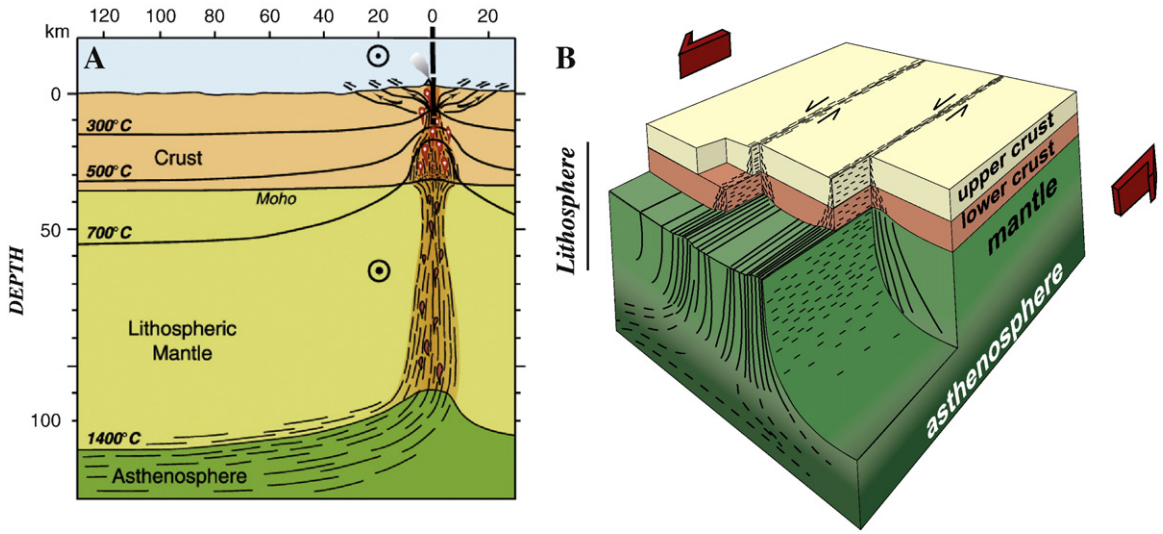

Fig. 4. Lithospheric faults: two schematic representations illustrating fault thickness variation with depth. In both cases the fault zone connects to the asthenosphere and deformation in the upper asthenosphere and lithosphere is mechanically coherent. (A) from Leloup et al. (1995) illustrates a concept of single lithospheric fault derived from the Ailao-Shan/Red Rover transcurrent fault; (B) from Vauchez and Tommasi (2003) after Teyssier and Tikoff (1998) illustrates a concept of transcurrent fault system merging to form a large-scale shear zone in the lithospheric mantle inspired from the San Andreas Fault system in western North America.

(Gourmelen and Amelung, 2005), southern Andes (Khazaradze et al., 2002), and western Mongolia (Vergnolle et al., 2003).

Major faults/shear zones probably affect the entire lithosphere. Although time scales and rheology for deformation in the brittle and ductile regimes differ strongly, a major fault zone (that crosscuts the entire lithosphere) should, on the long term, accommodate the same total offset close to the surface and in the deep parts of a lithospheric plate. Mechanical interactions between brittle and ductile deformations are therefore necessary to maintain compatibility along the fault (*e.g.*, Montesi, 2004). This raises the question of the mechanical behavior of the lithospheric mantle. Do "faults", *i.e.*, zones of localized strain, really exist in the mantle and, if so, how wide are they? Which are the mechanisms of localization in the mantle? Do they vary from the Moho to the lithosphere–asthenosphere boundary? What are the consequences of the development of a fault-related fabric on the physical properties of the lithospheric mantle?

2. Mantle deformation, crystal preferred orientations, and anisotropy

In contrast to the continental crust, the lithospheric mantle has a simple mineralogy dominated by olivine (50–80%), orthopyroxene (20–30%), and clinopyroxene (0–20%), with garnet, spinel, or plagioclase as minor phases (<5%). Deformation processes are relatively well constrained through the analysis of naturally deformed mantle rocks, deformation experiments, and geophysical data.

Seismology provides little evidence for brittle behavior in the lithospheric mantle. Precise relocation of earthquakes suggests there are very few seismogenic events at mantle depths with a few exceptions, beneath the Himalayas (Monsalve et al., 2009) or the East African Rift (Lindenfeld and Rümpker, 2011). These events were interpreted as resulting from specific processes such as flexure or dike-forming events related to the extrusion of kimberlitic or alkaline magmas. Observations from naturally deformed mantle peridotites also do not support brittle behavior under typical upper mantle pressure and temperature conditions.

Under typical upper mantle conditions, peridotites flow essentially through dislocation creep, which combines dislocation glide, climb and recrystallization, and thus requires a contribution of intracrystalline diffusion. At the crystal scale, dislocation glide occurs on a limited number of crystallographic planes and directions (slip systems), resulting in development of a crystal preferred orientation (CPO). The dominant slip system not only depends on the mineral structure, temperature, and strain rate, but also on pressure and water content. In minerals with few slip systems, like olivine and orthopyroxene, the dominant slip direction (Burgers vector) and slip plane tend to orient close to the flow direction and to the flow plane, respectively. The resulting CPO depends therefore on the available slip systems, their relative strength, which is a function of temperature, pressure, stress, and strain rate, and on the strain regime (*e.g.* Tommasi et al., 1999).

Transmission electron microscopy observations on naturally and experimentally deformed peridotites as well as deformation experiments on single-crystals indicate that under lithospheric conditions olivine deforms essentially by dislocation creep with dominant glide on {0kl}[100] systems (e.g. Bai and Kohlstedt, 1992; Bai et al., 1991; Demouchy et al., 2009; Doukhan et al., 1984; Durham and Goetze, 1977; Durham et al., 1977; Jung et al., 2006; Phakey et al., 1972). These observations are consistent with olivine CPO data in peridotite xenoliths and massifs (Ben Ismaïl and Mainprice, 1998): >90% naturally-deformed peridotites have their [100] axes either as a single maximum subparallel to the lineation or in a girdle within the foliation with a weak maximum subparallel to the lineation (Fig. 6). Naturally deformed olivine CPOs are consistent with those produced in simple shear and axial compression experiments in olivine aggregates at high temperature and moderate pressure (Bystricky et al., 2000; Nicolas et al., 1973; Zhang and Karato, 1995). They are also well-reproduced by polycrystal plasticity simulations that use slip systems data derived from high-temperature, low-stress deformation experiments on olivine crystals, that is, low critical resolved shear stresses on (010)[100] and (001)[100] systems (Tommasi et al., 2000; Wenk et al., 1991). The strength of olivine CPO does not vary linearly with finite strain. Starting from a random orientation, CPO intensity first increases rapidly, then progressively stabilizes, as dispersion associated with dynamic recrystallization counteracts CPO strengthening by dislocation glide (Fig. 7).

Preferred orientation of olivine crystals has important effects on the physical properties of the upper mantle. Elastic moduli, viscosity, electrical and thermal conductivities of the olivine crystal are anisotropic (*e.g.* Abramson et al., 1997; Durham and Goetze, 1977; Poe et al., 2010; Tommasi et al., 2001). Development of olivine CPO during deformation in the upper mantle results therefore in anisotropy of all these properties at the scale of the aggregate and at geophysically relevant scales if strain is coherent at those scales. Geophysical measurements of seismic anisotropy have been used to map the upper mantle deformation and strain repartition since the sixties (*e.g.*, Barruol et al., 1997b; Christensen, 1971; Hess, 1964; Mainprice et al., 2000; Nicolas and Christensen, 1987; Savage, 1999; Silver and Chan, 1991; Silver et al.,

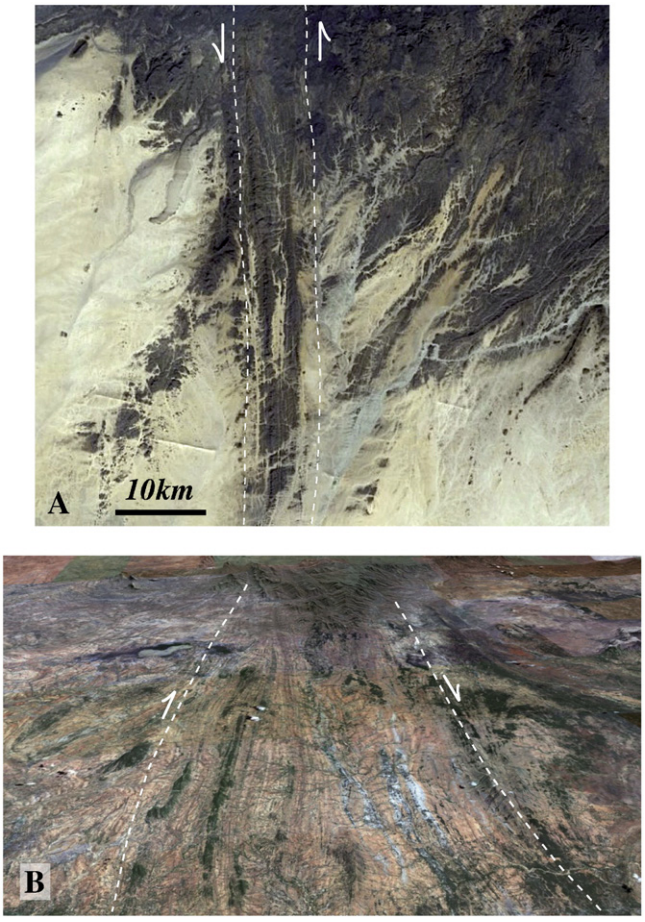

Fig. 5. Satellite views of two major transcurrent faults/shear-zones formed in the middle to lower crust. (A) ″4°50′ fault SW of Tamanrasset in the Hoggar massif, Algeria (from Google Earth-CNES/Spot Image-Digital Globe 2011). This neoproterozoic, ~10 km wide sinistral shear zone formed under amphibolite facies metamorphic conditions and was reactivated several times under decreasing temperature conditions (Caby and Andreopoulos-Renaud, 1987). Shear wave splitting measurements at Tamanrasset have evidenced a polarization of the fast S-wave parallel to the 4°50′ fault, *i.e.*, close to NS and a $\delta t \sim 0.9$ s (Barruol and Ismail, 2001). (B) Oblique view of the Antanimora dextral shear zone in the southern Madagascar neoproterozoic fault system (Google Earth-GeoEye 2011). This fault, >200 km long, comprises a ~25 km wide mylonite zone deformed under lower amphibolite to granulite metamorphic facies (Martelat et al., 1999).

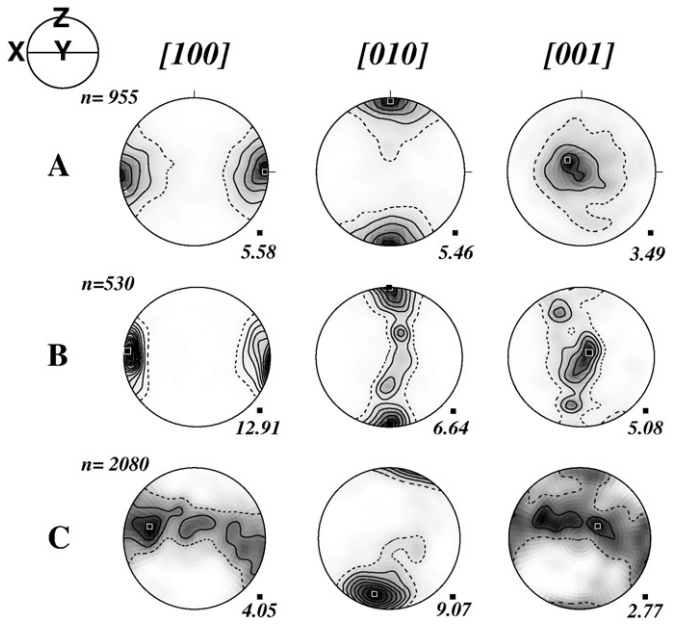

Fig. 6. The three most frequent crystallographic preferred orientation (CPO) of olivine in peridotites. (A) orthorhombic symmetry CPO characterized by three point maxima for [100], [010] and [001], this CPO results from dominant activation of the (010)[100] slip system. (B) [100]-fiber or [100]-axial symmetry CPO, characterized by a point maximum concentration for the [100]-axes and a dispersion of the [010]- and [001]-axes in a girdle with a [100] symmetry axis; this CPO results from the activation of multiple (0kl)[100] slip systems. (C) [010]-fiber or [010]-axial symmetry CPO with a point concentration of the [010]-axes and the [100]- and [001]-axes dispersed in a girdle with a [010] symmetry axes; this CPO results either from simultaneous activation of the [100] and [001] slip directions or from transpressional deformation. n is the number of measurements, XYZ are the main finite strain axes. The filled square and the value attached indicate the maximum concentration for each axis.

1999; Vauchez and Nicolas, 1991; Vinnik et al., 1992). Magnetotelluric data implying an anisotropy of electrical conductivity in the upper mantle has also been proposed as a tool to probe flow patterns in the lithospheric mantle and asthenosphere (*e.g.*, Jones et al., 1992; Mareschal et al., 1995). Finally, development of a coherent olivine CPO at large scales in the mantle results in an anisotropic thermal and mechanical behavior and thus influences subsequent deformation of the lithosphere. These aspects will be developed further on in this article.

3. Direct observations of shear zones and strain localization in the lithospheric mantle (location and details for all examples described in this section are presented in Table 1 and in the online supplementary material map).

The most straightforward evidence of strain localization in the lithospheric mantle comes from observations in peridotite massifs brought to the surface by orogenic processes and in oceanic lithosphere slabs obducted on continent margins (*e.g.*, Boudier et al., 1988; Dijkstra et al., 2004). In addition, xenoliths provide data on microstructures and CPO formed at various depths into the upper mantle.

3.1. Orogenic peridotites

Orogenic peridotite massifs provide direct sampling of the lithospheric mantle at scales ranging from tens of meters to tens of km. They are mainly composed by coarse-grained peridotites displaying a pervasive foliation and lineation outlined by a weak shape-preferred orientation of olivine (aspect ratios usually <1:3) visible in thin section only, spinel trails, and, sometimes, orthopyroxene alignment (*e.g.*, Nicolas et al., 1971; Reuber et al., 1982; Ross, 1977; Vissers et al., 1991). Compositional banding due to variations in the olivine–pyroxene proportion is also common and often, but not systematically, parallels the foliation. These coarse-grained peridotites systematically show well-developed olivine CPOs, consistent with deformation by dislocation creep involving dominant activation of {0kl}[100] systems (*e.g.*, Dijkstra et al., 2002a; Le Roux et al., 2008; Tommasi et al., 2006; Van der Wal and Vissers, 1996; Vauchez and Garrido, 2001). These observations are coherent with deformation under low stress conditions and imply that, if strain localization occurred, it took place at scales larger than the dimension of the massifs, that is, in "shear zones" at least tens of km wide.

"Classical" mylonitic shear zones were nevertheless mapped in the Ronda and Beni Bousera massifs in the Betic–Rifean belt, in S Spain and N Morocco (*e.g.*, Obata, 1980; Reuber et al., 1982; Tubia and Cuevas, 1987; Van der Wal and Vissers, 1996), Lanzo and Erro-Tobio in the Alps (*e.g.*, Nicolas et al., 1972; Vissers et al., 1995), Turon de la Técouère in the Pyrenees (Vissers et al., 1997), Horoman and Uenzaru in Japan (Furusho and Kanagawa, 1999; Sawaguchi, 2004). These shear zones are characterized by grain size reduction and by an apparent increase in finite strain relative to neighboring coarse-grained peridotites, suggested by the observation of highly-elongated orthopyroxenes (aspect ratios ≥1:10) marking the lineation, intrafolial folding, boudinage, and disruption of cm-scale pyroxenite layers (Fig. 8). Pressure and

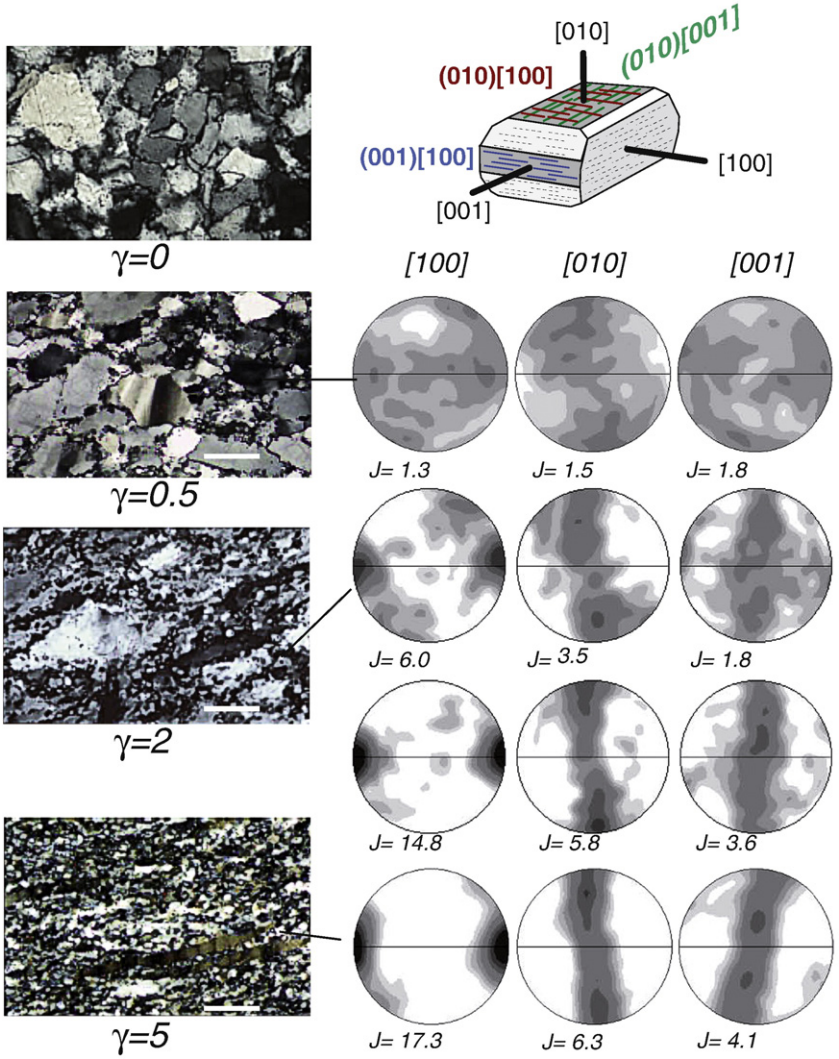

Fig. 7. Progressive evolution of the microstructure and texture (CPO) with increasing strain during torsion experiments on olivine aggregates (Bystricky et al., 2000) deformed at 6.3×10^{-5} s^{-1}, 1200 °C, 300 MPa confining pressure and oxygen fugacity near the Fe/FeO buffer (10^{-7} Pa). Shear sense is dextral, γ is the shear strain and the initial grain size is ~20 μm. The microstructure shows progressive stretching of crystals then dynamic recrystallization. The CPO shows a fast strengthening up to γ = 3–4 then tends to stabilize. The CPO shows a concentration of [100] close to the shear direction and a repartition of [010] and [001] in a girdle around the shear direction.

temperature conditions involved in the formation of the shear zones vary between the different massifs, but all record deformation under decreasing pressure and temperature conditions, probably associated with exhumation of the peridotites.

Strain localization at 65–70 km depth in a rather cold lithospheric mantle is recorded in shear zones a few hundreds of meters wide that form the external limits of the Ronda and Beni Bousera massifs in the Betic–Rif section of the Alpine belt in the western Mediterranean (Obata, 1980; Reuber et al., 1982). These shear zones are composed of mylonitic garnet-and-spinel lherzolites characterized by a bimodal olivine grain size distribution in which few relict porphyroclasts (0.5–1 mm long, aspect ratios attaining 1:5) are surrounded by a matrix of small recrystallized grains (~200 μm). Both porphyroclasts and recrystallized olivine grains present irregular shapes with sinuous grain boundaries, closely-spaced subgrain boundaries or undulose extinction and are elongated (recrystallized grains have aspect ratios of 1:2). Olivine and pyroxenes have well-developed CPO coherent with deformation by dislocation creep with dominant activation of (010)[100] in olivine and of {100}[001] and {110}[001] in pyroxenes (Soustelle et al., 2009). Detailed structural and petrological analyses of garnet–spinel mylonites from the Ronda massif support that mylonitization was coeval with decompression and cooling from *ca.* 1020–1100 °C at 2.4–2.7 GPa to 800–900 °C at 1.95–2.0 GPa (Garrido et al., 2011). These rocks therefore record localized strain and grain size reduction in the lithospheric mantle, but they display clear CPOs implying that this evolution did not trigger a change in dominant deformation mechanism from dislocation creep to grain boundary sliding. The actual thickness of the shear zones cannot be deduced from the study of these massifs, since they are bounded by the contact between the peridotites and the crustal rocks on one side and overprinted by higher temperature deformation on the other.

Hotter geotherms and lower pressures are inferred for the remaining examples. Structural mapping and analysis of the synkinematic mineralogy in the Erro-Tobio lherzolite (Voltri Massif, southern Alps) highlight progressive strain localization under decreasing temperature conditions, probably associated with mantle upwelling during Jurassic rifting and continental break-up (Vissers et al., 1991, 1995). Strain localization started in coarse-grained peridotites and resulted in the formation of a zone, at least one kilometer wide, of coarse-grained porphyroclastic peridotites with a uniform orientation of the foliation and lineation. The porphyroclastic microstructure of these "lherzolite tectonites" indicates extensive recrystallization through subgrain rotation and grain-boundary migration. Olivine CPO is consistent with dislocation creep with dominant activation of the (010)[100] slip system (Vissers et al., 1995). Thermobarometric estimates for these peridotites range from

Table 1
Location, age, rock type, microstructure and equilibrium temperature for the cited peridotite massifs, oceanic ophiolites and xenoliths.

	Locality	Geographic location	Age[a]	Lithologies	Microstructures and equilibrium PT conditions	Ref[b]
Orogenic peridotites	Ronda	Betic Cordillera, Spain	Early Miocene	sp-lherzolites and harzburgites, plg-lherzolites, minor gt-lherzolites and dunites, common pyroxenites	−gt + sp mylonites 1020–1100 °C, 2.4–2.7 GPa to 850 °C, 2 GPa −Porphyroclastic sp-peridotites: 900 °C −Coarse-grained, equigranular: 1100 °C −plg-bearing mylonites: 800–1000 °C, 1.1 GPa	1–6
	Beni Bousera	Rif Mountains, Morocco	Early Miocene	sp-lherzolites and harzburgites, minor gt-lherzolites and dunites, common pyroxenites	−gt + sp mylonites: 950–1000 °C, ~2 GPa −Fine- to coarse-porphyroclastic sp-peridotites: 1150–1100 °C, 1.7–1.8 GPa	7–8
	Lanzo massif	S Alps, Italy	Middle Jurassic/ Early Eocene	sp- and plg-lherzolites, minor harzburgites	−Coarse-porphyroclastic: 1100–1030 °C (cores) and 900–840 °C (rims), 1 GPa −Mylonites: 860–800 °C, 0.5 GPa	9–11
	Erro-Tobio	Voltri Massif, S Alps, Italy	Middle Jurassic/ Early Eocene	sp-lherzolites and harzburgites, minor dunites and pyroxenites	−Coarse-grained equigranular: 1030–1100 °C −Porphyroclastic: 920–1040 °C −Ultramylonites: 990–550 °C	12–14
	Turon de Técouère	Pyrenees, France	Early Cretaceous	sp- and plg-lherzolites	−Fine-porphyroclastic to ultramylonites: 900–650 °C	15–17
	Uenzaru	Hidaka belt, Hokkaido, Japan	Paleocene	sp- and plg-lherzolites, dunites, harzburgites	−Protomylonites: >960 °C, ~1 GPa −Mylonites: 760 °C, 0.7–0.8 GPa	18
Oceanic peridotites–ophiolites	Oman ophiolite, Basal shear zone	Oman	Early Cretaceous	Harzburgites	−Mylonites: 900 °C–1100 °C	19
	Oman ophiolite, Subvertical shear zones	Oman	Early Cretaceous	Dunites, harzburgites, and synkinematic gabbros	−Fine-porphyroclastic to mylonitic: ~1100 °C	20–21
	Red Hills ophiolite	New Zealand	Permian	sp-harzburgites and dunites	−Coarse-grained to porphyroclastic: 1050–750 °C	22
	Josephine ophiolite	Western USA	Middle Jurassic (~162 Ma)	Dominant harzburgites, dunites, wehrlites	−Coarse-porphyroclastic to mylonitic: 1100–900 °C	23–25
	Antalya ophiolite	Turkey	Late Cretaceous (~92 Ma)	Harzburgites, dunites, minor cpx-bearing harzburgites	−Coarse-porphyroclastic: >1000 °C −Mylonitic: ~800 °C?	26
	Othris ophiolite	Greece	Middle Jurassic (171 ± 4 Ma)	sp-lherzolites, harzburgites and dunites plg-lherzolites, amp-bearing harzburgites	−Coarse-porphyroclastic: 1200–1000 °C −Mylonitic to ultramylonitic: 900 °C to <780 °C	27
	Mirdita ophiolite	Albania	Middle Jurassic/ Middle Cretaceous	sp-lherzolite and -harzburgites plg-lherzolites, impregnated dunites	−Coarse-porphyroclastic: 1200–1000°C −Mylonitic: 1000–800 °C	28
	Lizard ophiolite	SW England	Devonian	sp-lherzolite and -harzburgites plg-lherzolites, impregnated dunites	−Coarse-porphyroclastic: 1200–1000 °C −Mylonitic: 1000–800 °C	29
	St. Paul's Rock	Equatorial Atlantic	Quaternary	Dunites	Porphyroclastic to fine-grained mylonitic	30
	Shaka Fracture Zone	SW Indian Ridge		sp-lherzolites and harzburgite, minor dunites	−Coarse-granular “tectonites”: 800–624 °C −Fine-grained mylonites: 671–577 °C	31
	West Santa Rosa Bank	Mariana trench	?	Dunites	−Coarse- to fine-grained porphyroclastic	32
Xenoliths	Persani Mountains	Southern Carpathians	Quaternary, Pleistocene	sp-lherzolites, subsidiary harzburgites	−Porphyroclastic: 950–1040 °C −Mylonitic to ultramylonitic: 850–940 °C, 0.9–1.7 GPa	33
	San Quintin	Baja California	Quaternary	sp-lherzolites, subsidiary harzburgites and dunites, minor pyroxenites	−Coarse-grained: 950–1050 °C, <2 GPa −Mylonitic: 800–950 °C, <1 GPa	34–35
	Montferrier	Southern France	Oligocene	sp-lherzolites, gt-clinopyroxenites	−Fine-grained porphyroclastic: 950 °C	36
	Tanlu fault	NE China	Neogene	sp-lherzolites, wehrlites, and minor pyroxenites	−Coarse-grained peridotites: 900–1050 °C −Mylonites: 750–900 °C	37
	Middle Atlas	Morocco	Middle and late Miocene to Quaternary	sp-lherzolites, harzburgites, wehrlites, sp(±gt)	−Coarse-grained peridotites: up to 1030 °C −Fine-porphyroclastic:	38

(continued on next page)

Table 1 (*continued*)

	Locality	Geographic location	Age[a]	Lithologies	Microstructures and equilibrium PT conditions	Ref[b]
				websterites, and clinopyroxenites	down to 830	
Xenoliths	Oran — Aïn-Temouchent volcanics	Western Algeria	Quaternary	sp- and sp + plg-lherzolites, subsidiary harzburgites	—Mylonites: ? —Coarse-grained harzburgites: 900–970 °C —Porphyroclastic lherzolites: 820–1080 °C —Mylonites: 870–930 °C	39
	San Andreas Fault	California W USA	Late Pliocene	lherzolites, harzburgites, wehrlites, dunites and clinopyroxenites	—Coarse-porphyroclastic: 970–1100 °C, 0.9–1.3 GPa	40

[a] Ages correspond to emplacement onto the crust for massifs and ophiolites and to extraction (volcanism ages) for xenoliths.

[b] References: 1: Obata (1980); 2: Van der Wal and Vissers (1996); 3: Tubia and Cuevas (1987); 4: Vauchez and Garrido (2001); 5: Soustelle et al. (2009); 6: Garrido et al. (2011); 7: Reuber et al. (1982); 8: Frets et al. (2012); 9: Nicolas et al. (1972); 10: Boudier (1978); 11: Kaczmarek and Tommasi (2011); 12: Vissers et al. (1991); 13: Hoogerduijn Strating et al. (1993); 14: Vissers et al. (1995); 15: Vissers et al. (1997); 16: Newman et al. (1999); 17: Newman and Drury (2010); 18: Furusho and Kanagawa (1999); 19: Boudier and Coleman (1981); 20: Boudier et al. (1988); 21: Michibayashi and Mainprice (2004); 22: Webber et al. (2010); 23: Kelemen and Dick (1995); 24: Warren et al. (2008); 25: Skemer et al. (2010); 26: Reuber (1984); 27: Dijkstra et al. (2002b); 28: Meshi et al. (2010); 29: Allerton and Macleod (1998); 30: Tilley (1947); 31: Jaroslow et al. (1996); 32: Michibayashi et al. (2009); 33: Falus et al. (2008); 34: Basu (1977); 35: Cabanes and Mercier (1988); 36: Cabanes and Briqueu (1987); 37: Ross et al. (1996); 38: J.M. Dautria (personal communication); 39: Zerka et al. (2002); 40: Titus et al. (2007).

1040 °C to 920 °C and ~1.4 GPa (Hoogerduijn Strating et al., 1993), which correspond to depths of 40–45 km and a relatively hot geotherm, supporting that this deformation occurred in the mantle during the early stages of extension (Vissers et al., 1995). Subsequent stages of strain localization led to formation of an anastomosed network (up to 200 m wide) of narrow shear zones in the southern part of the massif. These late shear zones are composed by mylonites in which ultrafine-grained bands (1–10 μm) anastomose around lenticular domains composed by partially recrystallized olivine porphyroclasts. Enrichment in amphibole in the ultrafine-grained bands allows to pinpoint deformation conditions to ~800–900 °C and highlights the implication of fluids in the latter stages of deformation. Continuation of deformation under still lower temperatures and with an increasing participation of fluids is suggested by crystallization of oriented antigorite, chlorite and tremolite in some mylonites.

Similar conclusions also hold for the Lanzo peridotite massif (Alps). Although essentially composed by coarse-grained porphyroclastic lherzolites, the Lanzo massif is crosscut by two NE-striking km-scale shear-zones (Boudier, 1978). Detailed structural investigation of the shear-zone that separates the northern and central Lanzo domains (Kaczmarek and Tommasi, 2011) highlights an asymmetric structure: the southern boundary is marked by a gradual rotation of the foliation in the porphyroclastic peridotites and by a progressive decrease in grain size, whereas the northern boundary is marked by a ~100 m wide, anastomosed network of mm-scale ultramylonite bands, followed by a sharp increase in grain size and foliation reorientation (Fig. 9). This evolution is consistent with progressive strain localization under decreasing temperature conditions leading to the formation of mylonites then ultramylonites at the expense of coarse porphyroclastic peridotites (compare with Fig. 3). Kaczmarek and Tommasi (2011) interpreted this shear zone as a mantle extensional fault (Fig. 9). Shearing in the hotter footwall was initially distributed in a wide shear zone (the present-day 1 km wide exposure represents only part of the initial high-temperature shear zone) formed under near solidus conditions. Exhumation along the shear zone was accompanied by cooling, leading to deformation under higher deviatoric stress, progressive strain localization, and grain size refinement. All microstructural facies display microstructures and olivine crystal preferred orientations consistent with dislocation creep with dominant activation of the (010)[100] system, although dynamic recrystallization results in larger dispersion of the CPO in the mylonites. Evidence supporting a change in dominant deformation mechanism from dislocation creep to grain boundary sliding, such as alignments of planar grain boundaries and very weak CPO, is limited to the anastomosed network of mm-scale ultramylonite bands where, solid-state reactions associated with the spinel- to plagioclase lherzolite transition resulted in development of a very fine-grained polyphase matrix.

Feedback between phase-transformation reactions and strain localization in the mantle was also proposed to play a role in the development of shear zones up to tens of meters wide within plagioclase-lherzolites in the Uenzaru peridotite in Japan (Furusho and Kanagawa, 1999) and in the southern part of the Ronda peridotite massif (Van der Wal and Vissers, 1996). In Ronda, for instance, strain tends to localize in more fertile layers and deformation seems to favor the spinel to plagioclase transformation. Newman et al. (1999) have studied in detail reaction-induced strain localization in the Turon de la Técouère peridotite massif in the Pyrenees. This small massif (~500 m wide) displays strongly foliated protomylonitic peridotites (<50% of fine-grained matrix), crosscut by mylonites (50–90% of fine-grained matrix) with similar foliation and lineation directions, but more shallowly dipping foliation. These mylonites are then intersected by a 25 m-wide layer of ultramylonites (>90% of fine-grained matrix; Vissers et al., 1997). Based on detailed analysis of the deformation microstructures, Newman et al. (1999) proposed that dislocation creep and dynamic recrystallization played an important role in the deformation of the coarser-grained domains, but that final grain comminution leading to the formation of the ultramylonites was controlled by syntectonic continuous net-transfer reactions associated with the spinel- to plagioclase-lherzolite transition. These reactions, which took place over a range of temperatures and pressures (750–950 °C and 0.5–1.1 GPa), produced fine-grained (2–25 μm) polyphase aggregates on the porphyroclast rims. The polyphase nature of these aggregates hindered grain growth, allowing a change in the dominant deformation mechanism from dislocation creep in the porphyroclasts to grain size sensitive creep in the very fine-grained matrix. Based on these observations, Newman et al. (1999) proposed that reaction-enhanced ductility may occur in the upper mantle wherever rocks move in pressure–temperature space, crossing phase boundaries. However, in a recent study, Newman and Drury (2010) nuanced this conclusion, proposing that the initial grain size may be crucially important for reaction-involved deformation, as it controls the surface area available for nucleation of new grains. Pre-existing variations in grain size, produced by dynamic recrystallization for instance, may therefore control the location and width of shear zones formed by reaction-softening.

In summary, observations in orogenic peridotite massifs suggest that, under high temperature, low-stress conditions, deformation in the mantle tends to be distributed over (or localized in) domains at least several tens of km wide (wider than the massifs outcropping scale). Evidence for progressive strain localization in shear zones tens of meters to 1–2 km wide is invariably related to deformation under decreasing pressure and temperature conditions (see Table 1). These shear zones are characterized by grain size reduction, which initially results from dynamic recrystallization. Analysis of the microstructures and crystal preferred

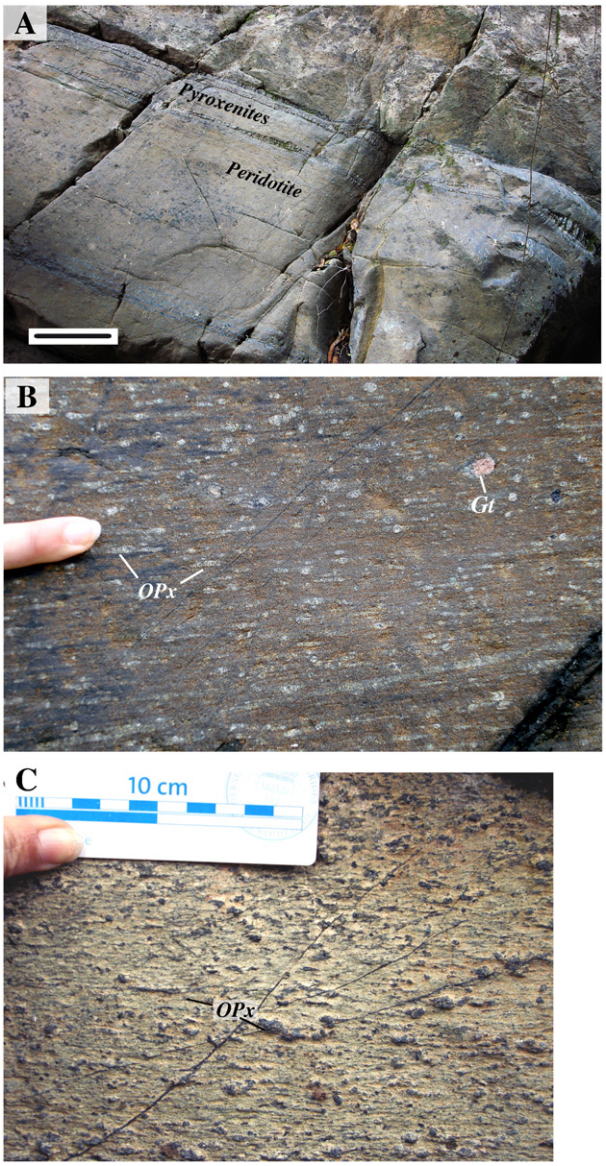

Fig. 8. Garnet-bearing mylonites from the Beni-Bousera massif (Rif, northern Morocco). (A) Outcrop showing the mylonitic foliation in the peridotite and boudinaged pyroxenite layers. Scale is 20 cm. (B) and (C) Details from the same mylonitic zone showing deformed garnet porphyroclasts (Gt) and very elongated orthopyroxene crystals (OPx). The groundmass consists of finely recrystallized olivine.

orientations of these mylonites attests however that grain size reduction through dynamic recrystallization does not lead to a change in dominant deformation mechanism from dislocation creep to grain boundary sliding. Microstructural evidence for grain boundary sliding is restricted to narrow (mm-scale) ultramylonitic bands concentrated in a 10 m- to 100 m-scale domains that form the coolest part of the shear zone, in which solid-state reactions associated with phase transitions or hydration allowed the crystallization of very fine-grained polyphase aggregates.

3.2. Strain localization in the oceanic lithosphere

Ophiolitic massifs are pieces of oceanic lithosphere obducted on continental margins. They provide therefore evidence on the strain repartition in the oceanic mantle. Similarly to orogenic peridotites, the mantle section of ophiolites is mainly composed by coarse-grained peridotites that display pervasive foliations and lineations interpreted as recording the asthenospheric flow beneath the ridge. The flow fabric was frozen during cooling and thickening of the oceanic lithosphere away from the ridge (*e.g.*, Nicolas et al., 1980). Localized deformation is nevertheless recorded in basal thrusts that accommodate the obduction of the ophiolite onto the continental margin (Boudier and Coleman, 1981), as well as in kilometric-scale shear zones that rework the "asthenospheric" fabric under high to moderate temperature conditions. Such shear zones have been mapped in many ophiolites, like the Oman (Boudier et al., 1988), Bay of Islands (Suhr, 1993), Antalya (Reuber, 1984), Othris (Dijkstra et al., 2002b), and Mirdita (Meshi et al., 2010) ophiolites. Smaller-scale (metric to decametric) high-temperature shear zones at high angle to the asthenospheric structures were also mapped in the Josephine ophiolite (Kelemen and Dick, 1995; Skemer et al., 2010; Warren et al., 2008).

In the Oman ophiolite, for instance, high-temperature shear zones trending parallel to the paleo-ridge, up to 2 km wide and 50 km long, affect peridotites and gabbros (Boudier et al., 1988). They are in structural continuity with the basal thrusts and are marked by abundant gabbroic synkinematic magmatism (Fig. 10). These observations suggest that this localized deformation is associated with the initial stages of the Oman ophiolite obduction. Based on a detailed analysis of the evolution of microstructures and olivine crystal preferred orientations in one of these shear zones, Michibayashi and Mainprice (2004) show that olivine CPO in the mylonites is partially inherited from the pre-existing, higher temperature fabric. Progressive mylonitization and accompanying grain size reduction results in dispersion of the olivine CPO and, in the central part of the shear zone, ultramylonites with almost random CPO are observed. CPO inheritance is also observed within cm-scale shear zones in the Red Hills ophiolite in New Zealand (Webber et al., 2010) and in decametric shear zones in the Josephine ophiolite (Skemer et al., 2010; Warren et al., 2008). This suggests that pre-existing mechanical anisotropy inherited from the higher temperature CPO formed at the ridge may control the tectonic behavior of oceanic mantle lithosphere during subduction and obduction.

Abundant synkinematic gabbros (Fig. 10) or microstructural evidence for synkinematic reactive melt transport is a characteristic feature of shear zones in ophiolites. It has been described in Oman (Boudier et al., 1988), Josephine (Kelemen and Dick, 1995), and in the Neothetysian ophiolites in the eastern Mediterranean domain (Dijkstra et al., 2002b; Meshi et al., 2010; Reuber, 1984). This implies that these shear zones formed at or close to the ridge, and highlights a feedback between deformation and melt transport. On the one hand, localized deformation in shear zones may increase the dynamic permeability of rocks; on the other hand, the presence of partially crystallized magmas weakens the shear zone. Further interaction between melt and deformation in an already cold oceanic lithosphere is evidenced by cross-cutting relationships between low-temperature peridotite mylonites and mafic dikes in the Lizard ophiolite (Southwest England), which were interpreted as recording synkinematic dike intrusion in an extensional shear zone (Allerton and Macleod, 1998). These authors propose: 1) that "gabbro mylonitic" zones weaken the oceanic lithosphere, and 2) have a high acoustic impedance contrast with the surrounding ultramafic rocks. They may therefore account for dipping seismic reflectors observed in the shallow oceanic lithosphere. Finally, development of amphibole-bearing mylonites, such as those mapped in the Lizard and Mirdita ophiolites (Allerton and Macleod, 1998; Dijkstra et al., 2002b; Meshi et al., 2010) or in the St. Paul's Rock in the equatorial Atlantic (Tilley, 1947), attests the focusing of fluids in some of these shear zones.

Strain localization in the sub-oceanic mantle lithosphere is also implied by mylonitic microstructures documented in *ca.* 14% of the abyssal peridotites dredged along fracture zones (Jaroslow et al., 1996; Warren and Hirth, 2006) and in mylonitic peridotites collected *in situ* in the West Santa Rosa Bank fault in the Mariana trench (Michibayashi et al., 2009). These mylonitic peridotites are characterized by strong grain size reduction, but dominant deformation by dislocation creep with activation of (010)[100] is nevertheless inferred from the analysis of the microstructures and olivine crystal preferred orientations in all samples (or sample domains) with grain sizes > 10 μm. Indeed, similarly to observations in

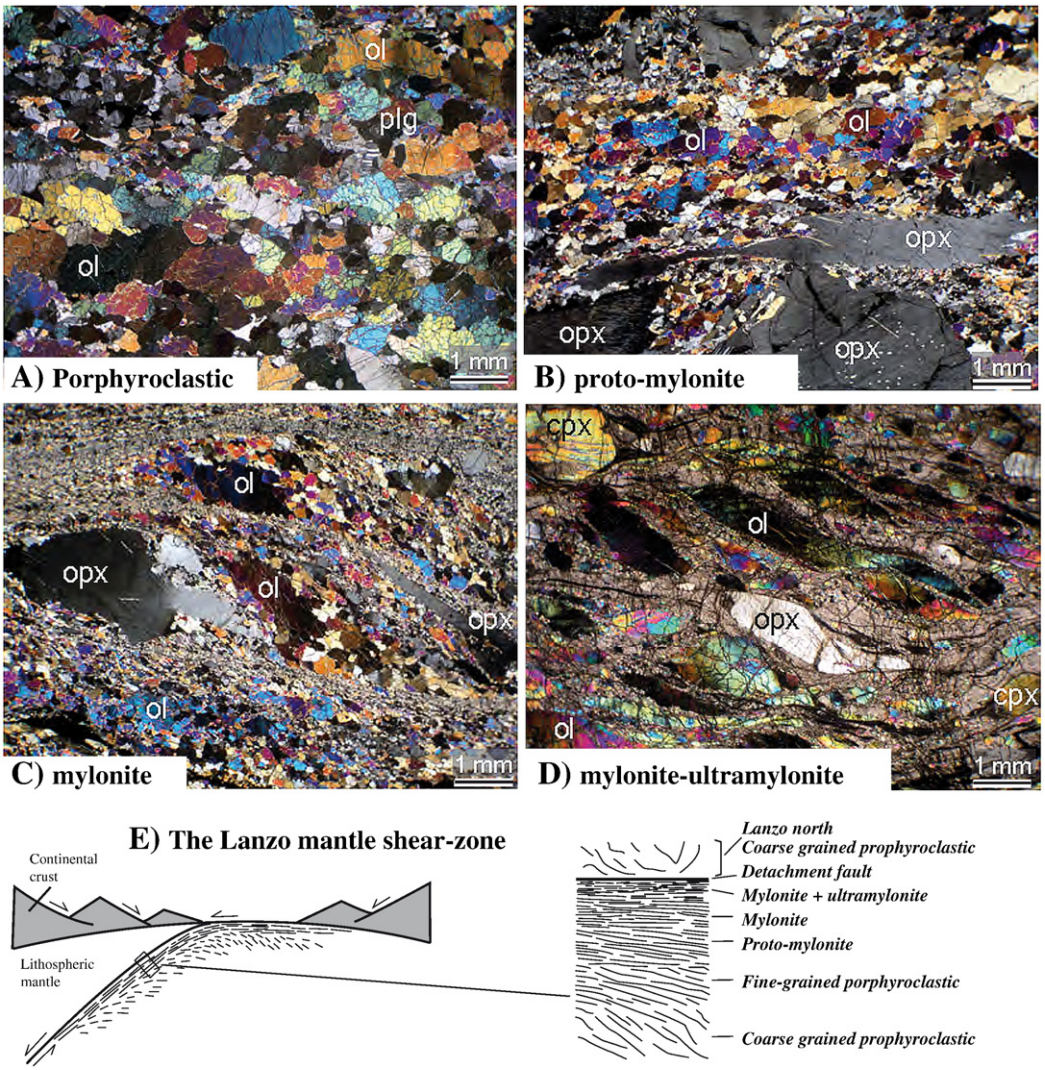

Fig. 9. Shear zone in the Lanzo massif (Alps) characterized by progressive grain comminution from fine-grained porphyroclastic to mylonitic with ultramylonitic band peridotites (A to D). Olivine progressively recrystallizes with finer grains toward the top of the exposed shear zone, orthopyroxene is elongated and partially recrystallized. This evolution suggests deformation under high stress conditions, probably due to decreasing temperature and was interpreted as reflecting the development of an extensional fault in the mantle (Kaczmarek and Tommasi, 2011). cpx = clinopyroxene; ol = olivine; opx = orthopyroxene; plg = plagioclase. (E) Cartoon showing a possible interpretation of the Lanzo mantle shear zone and the sequence of fault rocks as due to an extensional deformation (compare with Fig. 3).

orogenic massifs, evidence for a transition from dominant dislocation creep to grain boundary sliding is restricted to mm-scale bands of very fine-grained olivine–pyroxene (<5 μm) observed in some of these abyssal peridotites.

Finally, Nicolas and Boudier (2008) described an unusual type of large-scale "passive" shear zone in the Oman ophiolite. This shear zone puts in contact asthenospheric mantle (~1200 °C) with a ~1 Ma older lithospheric mantle (~1000 °C). Deformation and gabbro emplacement are restricted to the asthenospheric domain and shear senses vary from dextral to sinistral along the shear zone. Nicolas and Boudier (2008) interpreted this shear zone as resulting from channeling of asthenospheric flow, fed by a neighboring mantle diapir, along the "cold" lithospheric mantle boundary, the change in shear sense indicating that flow diverged from a neutral point determined by the proximity of the diapir. This peculiar "asthenospheric" shear zone results therefore from active mantle upwelling close to a transform or a ridge segment termination and probably does not represent a common situation. It is however interesting to consider that strain localization and development of preferred orientations may occur in the absence of relative motion of blocks at the surface.

In summary, observations in ophiolites indicate that km-scale shear zones develop in the suboceanic lithospheric mantle. The synkinematic magmatism associated with these shear zones together with their preferential orientation parallel or normal to the ridge trend suggest that they formed close to the ridge. This together with observations of structural continuity with the basal thrusts led many authors to propose that these shear zones formed during the early stages of the obduction. An alternative interpretation is that they represent transform faults. Analysis of the microstructures and olivine CPO in these shear zones as well as in mylonites dredged along major fracture zones indicates that dislocation creep with dominant activation of (010)[100] slip predominates. Similarly to what is observed in orogenic massifs, evidence for transition from dominant dislocation creep to grain boundary sliding is restricted to very fine-grained ultramylonite bands, for which a reaction-driven origin linked to melts or fluid percolation has been proposed (*e.g.*, Dijkstra et al., 2002b).

3.3. Mantle deformation: clues from xenoliths

Peridotite xenoliths have dominantly coarse-grained microstructures, which range from porphyroclastic to apparently undeformed coarse-granular. Average grain sizes are usually >1 mm and may attain >1 cm in the coarse-granular peridotites. Porphyroclastic peridotites are characterized by well-developed intracrystalline deformation

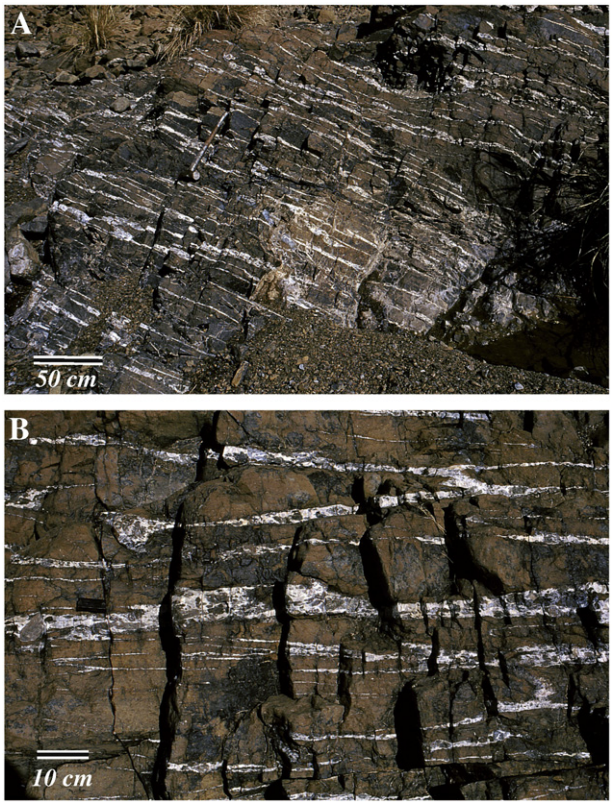

Fig. 10. Field pictures of synkinematic gabbros injected parallel to the mylonitic foliation of dunite in the Wadi Bulaydah (Miskin massif, Oman ophiolite; courtesy from F. Boudier). The shear zone was formed close to the ridge; it trends NE–SW, dips ~55 to 70° SE and bears a lineation oriented N170E.

features such as subgrains in olivine and kink bands in pyroxenes, as well as by a weak shape preferred orientation due to elongation of olivine crystals. Grain size distribution in porphyroclastic peridotites may be bimodal, and thus characteristic of dynamic recrystallization. This is however not systematic and seems to be more frequent for samples from the shallow mantle. In many cases, the absence of bimodal distribution together with the sinuous character of olivine grain boundaries, suggest that grain boundary migration allowing for synkinematic grain growth is common. Such microstructure supports that deformation under low deviatoric stress conditions tends to predominate in the lithospheric mantle. Coarse-granular peridotites (protogranular peridotites from Mercier and Nicolas, 1975) do not display shape preferred orientations or intracrystalline deformation features, but their strong olivine CPO, similar to those usually measured in porphyroclastic peridotites, indicates that they have been deformed through dislocation creep; their apparent undeformed texture results essentially from post-deformational annealing.

Formation of mylonites at the expenses of spinel-bearing peridotites through extensive grain size refinement due to dynamic recrystallization is only observed in a few basalt-borne xenolith localities: the Persani Mountains in the southern Carpathians (Falus et al., 2008), the San Quintin volcanic field in Baja California (Basu, 1977; Cabanes and Mercier, 1988), Montferrier in southern France (Cabanes and Briqueu, 1987), the Tanlu fault in NE China (Ross et al., 1996), the Middle Atlas in Morocco (J.M. Dautria, personal communication), and the Oran volcanics in Algeria (Zerka et al., 2002). Even in these suites, coarse-grained textures predominate; mylonitic and ultramylonitic textures usually represent <20% of the sampled xenoliths. An exception is the San Quintin suite, where >75% of the xenoliths are mylonitic (Basu, 1977; Cabanes and Mercier, 1988).

From these examples, the southern Carpathian xenoliths are particularly interesting because they display an almost continuous variation in microstructure, characterized by increase in the volume of recrystallized grains and decrease in recrystallized grain size, which ranges from 80–300 μm in the coarser mylonites to 40–60 μm in the most recrystallized peridotites (Falus et al., 2008). Recrystallized grains often display evidence for internal strain and are elongated subparallel to the lineation defined by the elongation of porphyroclasts. Their boundaries are usually curvilinear, except for the finest grains in the mylonites, which display polygonal shapes with straight or gently curved boundaries. These observations together with well-developed olivine CPO point to deformation accommodated essentially by dislocation creep with dominant activation of {0kl}[100] slip systems. Dynamic recrystallization is nevertheless accompanied by a dispersion of the olivine CPO, which is proportional to the volume fraction of recrystallized grains (Falus et al., 2011).

Strong shearing under high stress conditions has also been inferred for lherzolite mylonites with fluidal microstructures from kimberlites (Boullier and Nicolas, 1975). However the processes allowing for grain size reduction and strain localization at the high temperatures at which these mylonites are equilibrated (Boyd, 1973) are still poorly understood. Gueguen and Nicolas (1980) have, for instance, proposed that these rocks record the early stages of the diapiric upwelling of kimberlites rather than plate tectonics or convection-related deformation.

To conclude, if we assume that xenolith sampling is representative of the relative proportion of the various types of microstructure in the lithospheric mantle, the rarity of mylonitic and ultramylonitic peridotite xenoliths suggests that strain localization associated with grain size reduction remains an infrequent phenomenon that affects small volumes in the shallow lithospheric mantle. Almost all mylonite-bearing xenolith localities are located along large-scale faults, which often display a strike-slip component of deformation. One should nevertheless note that xenoliths from the lithospheric mantle beneath the San Andreas Fault system in California display a coarse-grained microstructure and rather strong olivine CPO (Titus et al., 2007), suggesting low work rates and hence that the strong velocity gradient beneath this major plate boundary is accommodated over a wide zone in the lithospheric mantle. The nature of xenolith sampling implies, however, that strain localization at low temperatures, giving rise to highly heterogeneous microstructures characterized by mm-scale ultramylonitic bands similar to those observed in peridotite massifs, cannot be excluded. Such ultramylonitic bands would represent weaknesses along which fracturing during xenoliths extraction would preferentially take place and the fine-grained microstructure in these bands would favor reaction with the magma. Together, these two processes imply that ultramylonitic bands have a low probability to be preserved in xenoliths.

4. Geophysical evidence of fault continuation into the lithospheric mantle

A crucial issue with peridotite massifs and xenoliths is that they represent pieces of lithospheric mantle with variable sizes (very small in the case of xenoliths) that have been extracted from their initial location in the mantle by either tectonic or magmatic processes. Most times, the *in situ* geometry has been lost and the lateral extension of the processes cannot be constrained. Their representativeness needs therefore to be evaluated by independent approaches. Geophysical imaging of the Earth interior has the potential of providing *in situ* evidence that major fault zones penetrate the lithospheric mantle. However, interpreting these indirect observations in terms of geological processes is, in most cases, not straightforward.

4.1. Moho offsets, mantle reflectors, and velocity discontinuities

Seismic profiling provided many examples of Moho offsets and sub-crustal reflectors aligned with the trace of crustal faults, suggesting that these faults penetrate the mantle. Some of the earliest and most famous observations come from the BIRPS experiments that,

in the 1980s, imaged mantle reflectors in the British Caledonides, like the shallowly-dipping Flannan reflector, interpreted as an extensional fault in the shallow lithospheric mantle, or the Moho offset below the Great Glen Fault, regarded as evidence of reactivation of this major Caledonian transcurrent fault during the opening of the North Atlantic (Brewer et al., 1983; Smythe et al., 1982). More recent profiles (McBride et al., 1995; McGeary and Warner, 1985; Reston, 1990) confirm the existence of mantle reflectors and image several Moho offsets aligned with asymmetric half-grabens in the North Sea (Fig. 11A) suggesting that extensional fault zones accommodating the opening of the North Atlantic crosscut the crust–mantle boundary and penetrate several tens of kilometers into the lithospheric mantle. Sea-dipping reflectors ~10 km below the Moho were also imaged by wide-angle reflection profiles west of Norway (Mjelde and Sellevoll, 1993). Modeling of P-to-S conversions produced by these reflectors requires an anisotropic uppermost mantle with fastest P-wave propagation along a direction inclined at 45° to the horizontal, consistent with shearing in normal faults accommodating post-Caledonian extension. A 5 km Moho offset associated with a near-vertical, non-reflective zone (5–10 km in width) in the lower crust imaged by deep seismic reflection profiling in southern Urals was also interpreted as a fault zone penetrating in the uppermost mantle (Diaconescu et al., 1998), indicating that these structures are not an exclusivity of continental margins.

Regional seismic tomography also shows sharp velocity contrasts in the lithospheric mantle below major transcurrent fault zones such as the Altyn Tagh Fault in Tibet (Wittlinger et al., 1998) or the South Armorican shear zone in the Hercynian belt in Brittany (Judenherc et al., 1999). Receiver function analysis provides additional evidence for Moho offsets beneath Tibet and adjacent areas (Ai et al., 2005; Kind et al., 2002; Shi et al., 2004; Wittlinger et al., 1998), in Alaska (Ai et al., 2005), and in the Arabian shield (Levin and Park, 2000). Finally, receiver function imaging of the lithosphere–asthenosphere boundary (LAB) beneath eastern China highlights that the maximum LAB upwelling in this area occurs below the surface expression of the Tanlu fault, suggesting that this major active strike-slip fault zone affects the entire lithosphere and that its reactivation played a major role in the thinning of the North China craton in the Mesozoic–Cenozoic (Chen et al., 2006).

Moho offsets and mantle reflectors are also observed below cratons. Seismic profiles in the Gulf of Bothnia in the Baltic shield, for instance, show a 10 km Moho offset linked to a reflector extending from the lower crust into the mantle, which was interpreted as a thrust fault (BABEL Working Group, 1990). Shallowly dipping reflectors were recorded in the Slave craton in Northern America by reflection profiles

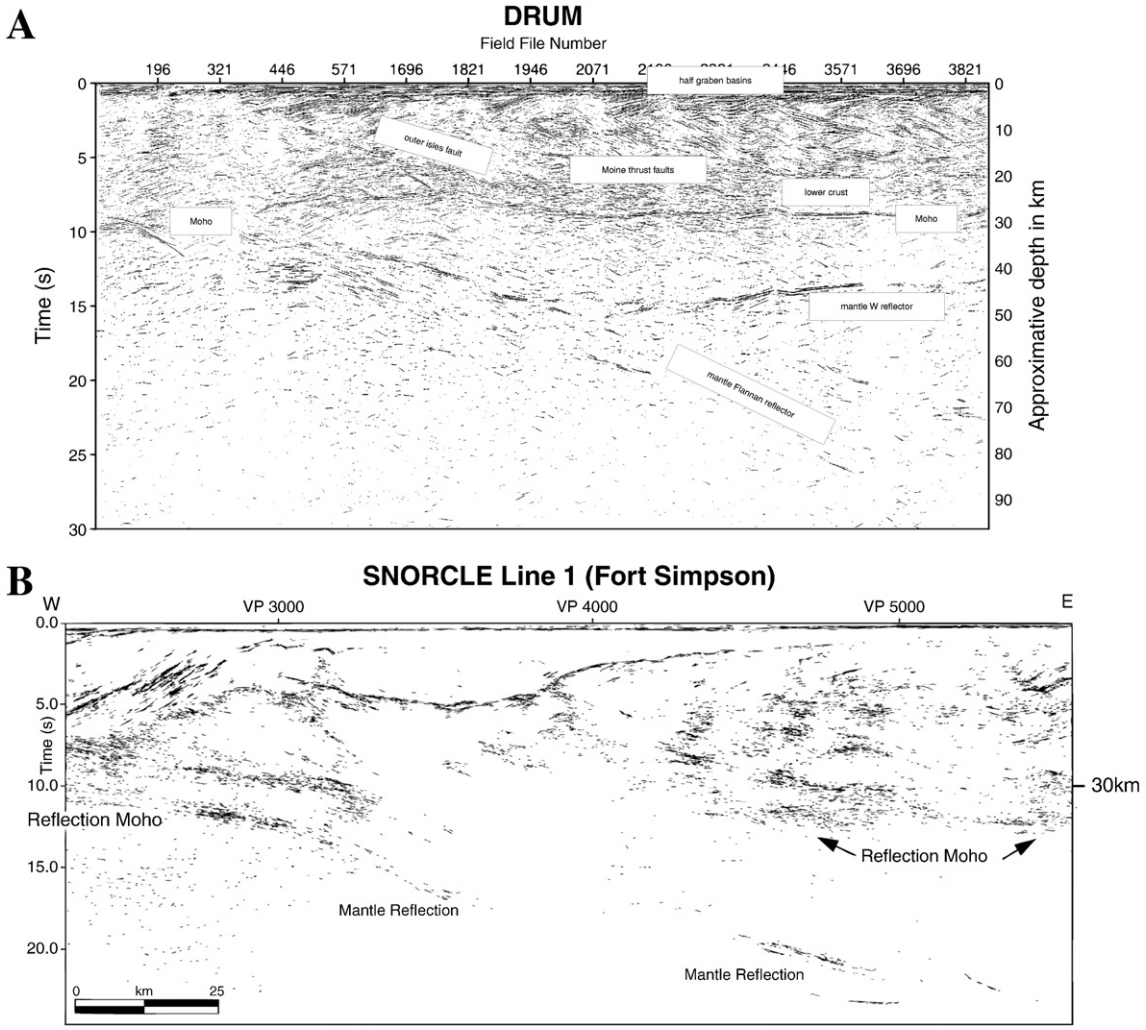

Fig. 11. Mantle reflectors in seismic reflection profiles. In both profiles data are migrated and filtered and are presented in vertical two-way travel time. (A) The DRUM (Deep Reflections from the Upper Mantle) seismic reflection annotated profile (http://www.earthscrust.org/science/transects/drum_scotland.html). This profile displays several reflectors below the seismic Moho, especially the Flannan reflector, interpreted either as a normal or a thrust fault, and the still poorly understood W reflector. Normal faults in the crust bound asymmetrical extensional basins and dip in the same direction as the Flannan reflector. (B) Seismic reflection data from the SNORCLE Line 1 in the Fort Simpson area (Cook et al., 1999) in the Slave craton of Canada. The shallower reflector on the right was interpreted by Bostock (1999) as a 10 km thick layer exhibiting 5% anisotropy.

(Fig. 11B; Cook et al., 1999) and receiver function data. Based on the analysis of P-to-S converted phases, Bostock (1997, 1998) proposed, for instance, an anisotropic stratification of the lithospheric mantle below the Slave craton with major boundaries at 75, 135, and 195 km depth. The shallowest, best-defined reflector at 75 km depth was interpreted as a shallowly-dipping, 10 km thick layer with a sharp upper interface (~400 m) and a diffuse lower boundary (>2 km) and ~5% internal anisotropy. These characteristics are in good agreement with those expected from an asymmetric shear zone, like the one mapped in northern Lanzo for instance. Coupling receiver functions and surface wave azimuthal anisotropy also allowed to image deep seismic discontinuities in the subcratonic lithospheric mantle. In the Slave craton, Snyder (2008) detected shallowly dipping discontinuities with a mild anisotropy at 120–130 km and 170 km depth. Mid-lithospheric discontinuities at depths between 60 and 170 km were also mapped beneath the Superior craton and the Canadian Shield (Miller and Eaton, 2010; Rychert and Shearer, 2009). A strong change in Rayleigh azimuthal anisotropy pattern at depths varying laterally from 60 to 150 km is also observed in these cratons (Yuan and Romanowicz, 2010). The geological nature of these discontinuities within the cratonic mantle is however poorly constrained. They might represent fossil shear zones that put into contact domains with different compositions and tectonic histories during the formation of these cratonic roots or remnants of slabs accreted to the cratonic roots during plate convergence episodes (Miller and Eaton, 2010; Snyder, 2008).

4.2. Seismic anisotropy

As discussed in previous sections, analysis of naturally deformed peridotites suggests that shearing in the upper mantle occurs essentially by dislocation creep, leading to development of olivine crystal preferred orientations and hence to a strong anisotropy of the elastic properties of peridotites (Christensen, 1971; Mainprice and Silver, 1993; Mainprice et al., 2000; Nicolas and Christensen, 1987). Seismic anisotropy measurements, especially shear wave splitting, but also Pn or Rayleigh wave azimuthal anisotropy, may therefore provide additional clues about the continuation of major faults within the lithospheric mantle (*cf.* reviews by Silver et al., 1999; Vauchez and Tommasi, 2003).

Most shear wave splitting measurements are performed using teleseismic radially-polarized S-waves (SKS, SKKS, PKS…) that propagate from the core–mantle boundary (CMB) to the seismic station with a steep, almost vertical incidence (Fig. 12). In an anisotropic upper mantle, the S-wave is split into two orthogonally polarized components that propagate at different velocities. The fast split shear wave is polarized in a plane defined by the propagation direction and the direction in which most [100] olivine axes (*a*-axes) are aligned (Fig. 12C). For "normal" lithospheric mantle conditions (*i.e.*, at medium-high temperature, moderate pressure, and H_2O "poor" compositions), dislocation creep tends to progressively orient olivine [100] axes close to the flow direction (kinematic lineation; Fig. 12B). The direction in which the fast split S-waves are polarized

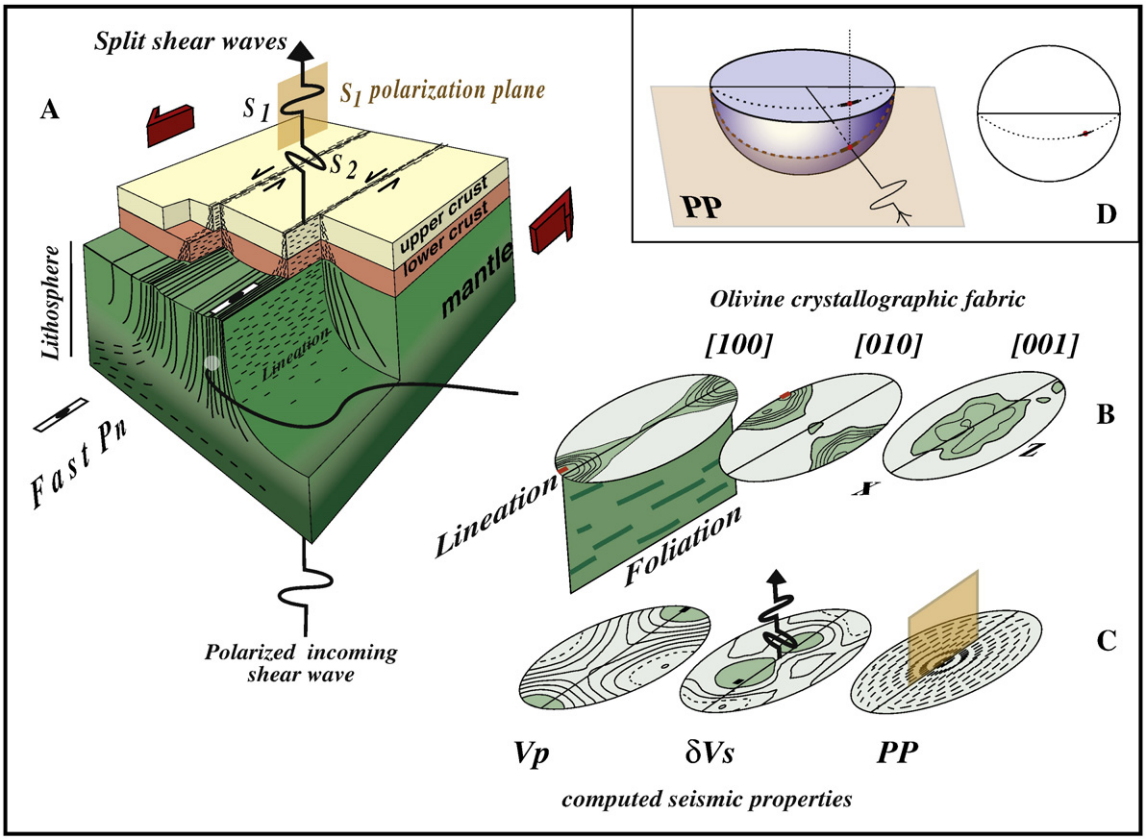

Fig. 12. Shear wave splitting in a transcurrent fault zone affecting the whole lithospheric mantle thickness (A). On this figure, a vertically incident polarized SKS wave propagates through a lithospheric mantle with a vertical foliation bearing a horizontal lineation. Transcurrent simple-shear causes the development of an olivine CPO (B) with [100] close to the lineation, [010] close to the normal to the foliation plane, and [001] orthogonal to the lineation in the foliation plane (orthorhombic symmetry). Panel (C) shows in the same structural referential the 3D seismic properties computed for this olivine CPO. The *Vp* diagram shows the highest P-wave velocity close to the maximum concentration of [100]-axis; the δ*Vs* diagram shows the velocity difference between the fast and slow split S-waves for all propagation directions; the maximum birefringence is for S-waves propagating in a direction almost normal to the lineation, *i.e.*, with a subvertical incidence in the case shown in (A). The *PP* diagram shows the orientation of the plane in which the fast S-wave is polarized; this plane is consistently defined by the fast S-wave propagation direction and the direction of the maximum concentration of [100]-axes (lineation). Panel (D) shows how the polarization plane is represented in a stereographic projection: to maintain lisibility only a small segment of the intersection between the polarization plane and the lower hemisphere projected on the equatorial plane is shown.

is therefore indicative of the flow direction. The delay time between the arrivals of the fast and slow S-waves depends on the thickness of the anisotropic layer and on its apparent anisotropy that, in turn, depends on the CPO strength and on the propagation direction of the seismic wave relative to the olivine CPO.

S-wave splitting measurements have therefore the potential to sample the upper mantle deformation and hence could provide evidence of the continuation of major fault zones into the lithospheric mantle. Main limitations are:

1) The intrinsic S-wave polarization anisotropy of mantle rocks is not high (in most cases maximum anisotropies range between 4 and 7%). Wave paths within a "homogeneous" anisotropic layer have thus to be long enough to generate a significant, *i.e.*, reliably measurable, delay time between the arrivals of the fast and slow S-waves. As a rule of thumb, a 100 km thick anisotropic upper mantle produces ~1 s delay time. Delay times <0.3 s are difficult to characterize using teleseismic waves and may also result from anisotropy in the crust (Barruol and Mainprice, 1993; Crampin, 1984; Herquel and Wittlinger, 1994; McNamara et al., 1994). This means that anisotropic layers should attain a vertical extent of several tens of kilometers to be "visible" in teleseismic data.
2) The lateral extent of the anisotropic domains should be larger than the wavelength of the waves used for measurement; otherwise the seismic wave averages the elastic properties of the various sampled domains. Lateral homogeneity over ~50 km is considered as a suitable value when analyzing teleseismic shear wave splitting (Alsina and Snieder, 1995). Finite frequency analysis techniques applied to dense seismic arrays may however allow detection of lateral variations in anisotropy on the scale of 10–20 km if good azimuthal coverage is available (Chevrot, 2006).
3) Any anisotropic layer traversed by a S-wave affects its polarization. For teleseismic S-waves, the splitting observed at a seismic station represents an integral along the ray path on the receiver side from the CMB to the station. Petrophysical data suggest that the anisotropy is mostly localized in the upper mantle (*cf.* review in Mainprice et al., 2000). Analysis of surface waves anisotropy tends to reduce this domain to approximately the first 200 km of the upper mantle, *i.e.*, the lithospheric mantle and the asthenosphere (Debayle et al., 2005; Montagner and Kennett, 1996; Savage, 1999). The vertical repartition of the seismic anisotropy may be approached indirectly by determining whether the observed signal is better explained by the presence of two layers of anisotropy rather than by a single one beneath the station, but this requires splitting measurements performed on teleseismic S-waves from a large range of azimuths (Rümpker and Silver, 1998; Silver and Savage, 1994).

These three points limit the use of S-wave splitting to determine the presence of mantle faults at depth. If strain is localized in thin zones (<tens of km wide) or if olivine crystal preferred orientation is too weak, mantle shear zones will not produce a measurable S-wave splitting. Shallowly-dipping shear zones will be harder to detect than steeply-dipping ones, since in the former an almost vertically propagating S-waves will cross the shear zone at high angle, while in a steeply-dipping shear zone it will propagate along the shear zone and the anisotropic path may be as long as the vertical extent of the fault.

S-wave splitting measurements have nevertheless provided strong evidence for the persistence of major faults into the lithospheric mantle. Active transform plate boundaries are choice targets for such studies since they are expected to affect the entire lithosphere. The San Andreas Fault system in western North America is one of the most studied transform boundaries with a dense seismological network in California allowing a reliable determination of shear wave splitting parameters (Fig. 13). By analyzing the dependence of the measured splitting parameters on the core-refracted S-wave back-azimuth, Ozalaybey and Savage (1994) and Silver and Savage (1994) have shown that, at stations close to the San Andreas Fault, the measured splitting results from the summation of the effects of two anisotropic layers, where the upper layer (equated to the lithosphere) is characterized by a polarization of the fast S-wave parallel to the trace of the San Andreas Fault system. Subsequent S-wave splitting measurements in this region (Bonnin et al., 2010; Hartog and Schwartz, 2001; Ozalaybey and Savage, 1995) confirmed this conclusion (Fig. 13B), suggesting that the fault system crosscuts the entire lithosphere. This interpretation is also consistent with faster NW–SE Pn propagation directions beneath central western California (Hearn, 1996) and with recent geochemical data showing that rocks exposed along the San Andreas Fault retained evidence of percolation and reaction with fluids that have isotopic compositions supporting mantle-derived origin (Pili et al., 2011). By analyzing S-wave splitting on a dense network, Bonnin et al. (2010) concluded that the San Andreas Fault system is composed by several faults *ca.* 40 km wide that add up to form a lithospheric-scale transcurrent system at least 130 km wide at the base of the lithosphere (~70 km deep). Rayleigh wave azimuthal anisotropy in western California also suggests transcurrent deformation distributed over a 100–200 km wide domain in the lithospheric mantle (Lin et al., 2009).

Splitting measurements at the Caribbean–South America plate boundary (Growdon et al., 2009; Russo et al., 1996) and above the Alpine Fault in New Zealand (Duclos et al., 2005; Klosko et al., 1999; Marson-Pidgeon et al., 1999) show fast polarization directions parallel to the trend of these transform boundaries and high delay times (>1.4 s with values ≥2 s) at the stations close to the major strike-slip faults that compose these plate boundaries. Variation in splitting parameters with back-azimuth, indicating variation in anisotropy with depth, is not observed. The delay times >2 s imply indeed fault-parallel flow directions in the entire lithospheric mantle and in the asthenosphere beneath both transform boundaries. In the Caribbean, roll-back of the subducting Atlantic plate is proposed to produce E–W shearing in the asthenospheric mantle, which adds up to the strike-slip deformation in the lithospheric mantle beneath the El Sebastian–Pilar fault system that marks the plate boundary in the region (Growdon et al., 2009). In New Zealand, analysis of the lateral variation of splitting parameters coupled to P-wave anisotropy data on both sides of the Alpine Fault led Duclos et al. (2005) to propose that the shear zone is rather narrow at the Moho depth, but widens quickly downward and might be as wide as the South Island (>150 km) in most lithospheric mantle, and possibly wider in the asthenosphere.

Fault-parallel fast S-wave polarizations are also usually observed beneath major intra-continental transcurrent faults, both active, as the Kunlun fault in Tibet (McNamara et al., 1994) and the Dead Sea fault (Rümpker et al., 2003), or fossil, like the neoproterozoic Alem–Paraiba fault in South America (Assumpcao et al., 2006; Heintz et al., 2003) or the Caledonian Great Glen Fault in the Scottish Highlands (Bastow et al., 2007). In many cases, the polarization of the fast split shear wave changes abruptly from oblique to parallel to the fault trend approaching the surface expression of the fault. This rotation of the fast S-wave polarization is usually consistent with the kinematics of the fault and was interpreted as marking a re-orientation of olivine crystals due to strike-slip deformation in the mantle. It is thus regarded as a strong argument supporting crust–mantle mechanical coupling in these faults. S-wave splitting measurements across the dextral Kunlun and sinistral Altyn Tagh faults in the Himalayan orogen (Herquel et al., 1999; McNamara et al., 1994) show, as one approaches the fault, respectively a clockwise and an anticlockwise rotation of the fast wave polarization to parallelism with the trend of the fault (Fig. 14B). Delay times of 1 s beneath the western part of the Altyn Tagh Fault suggest that the entire lithosphere is affected by the transcurrent deformation (Herquel et al., 1999; Li et al., 2011). Higher delay times, reaching 2 s, are observed beneath the Kunlun fault (McNamara et al., 1994). Additional evidence for a

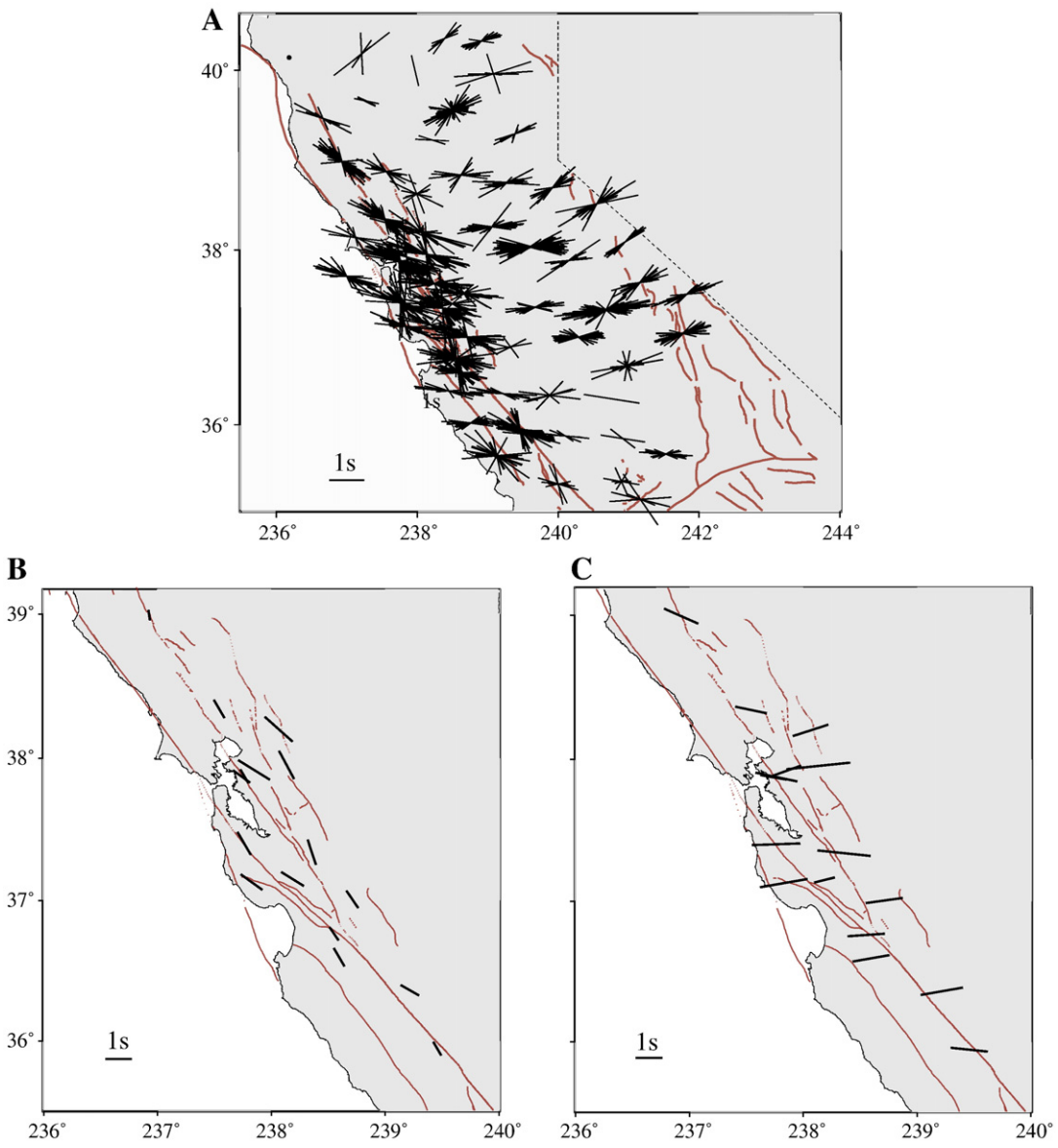

Fig. 13. Shear wave splitting in the San Andreas Fault area (Bonnin et al., 2010) and 2-layer model. Panel (A) shows the apparent anisotropy obtained from selected good measurements over the studied area, and the dispersion of the fast split wave polarization direction. Panels (B) and (C) show the results of the best fitting 2-layer model obtained at several stations. The upper layer (lithosphere, B) displays a polarization of the fast S-wave parallel to the San Andreas Fault system, instead the lower layer (asthenosphere, C) requires an almost EW polarization of the fast S-wave.

mantle-penetrating Altyn Tagh Fault is provided by regional seismic tomography in northern Tibet that shows a low-velocity anomaly located just beneath the surface expression of the fault (Fig. 14A); this anomaly separates two seismically distinct domains and was interpreted as a ~40 km-thick mantle shear zone (Wittlinger et al., 1998). Approaching the north-eastern termination of the Altyn Tagh Fault, the fault geometry changes and fast S-wave polarization oblique to the fault are observed (Li et al., 2011). This pattern suggests that fault penetration is restricted to the crust in this domain. This inferred along-fault change in geometry is consistent with quaternary mantle-derived magmatic events limited to the south-western part of the fault (Li et al., 2011). Finally, in north-eastern Tibet, stations above major (block-limiting) faults show a simple anisotropy pattern, characterized by fault-parallel polarizations and delay times >1 s, whereas stations located between the faults show a two-layer anisotropy with an ENE upper layer polarization, interpreted by Li et al. (2011) as recording the crustal deformation, and a WNW lower layer polarization, interpreted as recording diffuse deformation of the lithospheric mantle (Fig. 14B).

In contrast, recent splitting measurements in Central Iran showed fast split shear waves consistently polarized parallel to the structural trend of the Alpine collisional belt, at large angle from the absolute plate motion (Kaviani et al., 2009). This pattern is consistent with dominant orogen-parallel shearing in the lithospheric mantle, suggesting transpressive deformation (Tommasi et al., 1999; Vauchez and Nicolas, 1991). Transpression is also inferred from the surface deformation field deduced from GPS data, which highlights orogen-parallel displacement along transcurrent faults (Vernant et al., 2004). The good correlation between GPS data, shear-wave splitting measurements, and surface geology points to a mechanically coherent deformation of the entire lithosphere. However, deformation at the surface is strongly localized in major strike-slip faults, whereas seismic anisotropy measurements suggest distributed deformation in the mantle beneath this active convergent plate boundary emphasizing a very strong depth-dependent mode of deformation. The homogeneous seismic anisotropy over a wide area might, however, result from the integration of the signal of multiple closely-spaced belt-parallel transcurrent shear zones (*e.g.*, Bonnin et al., 2010).

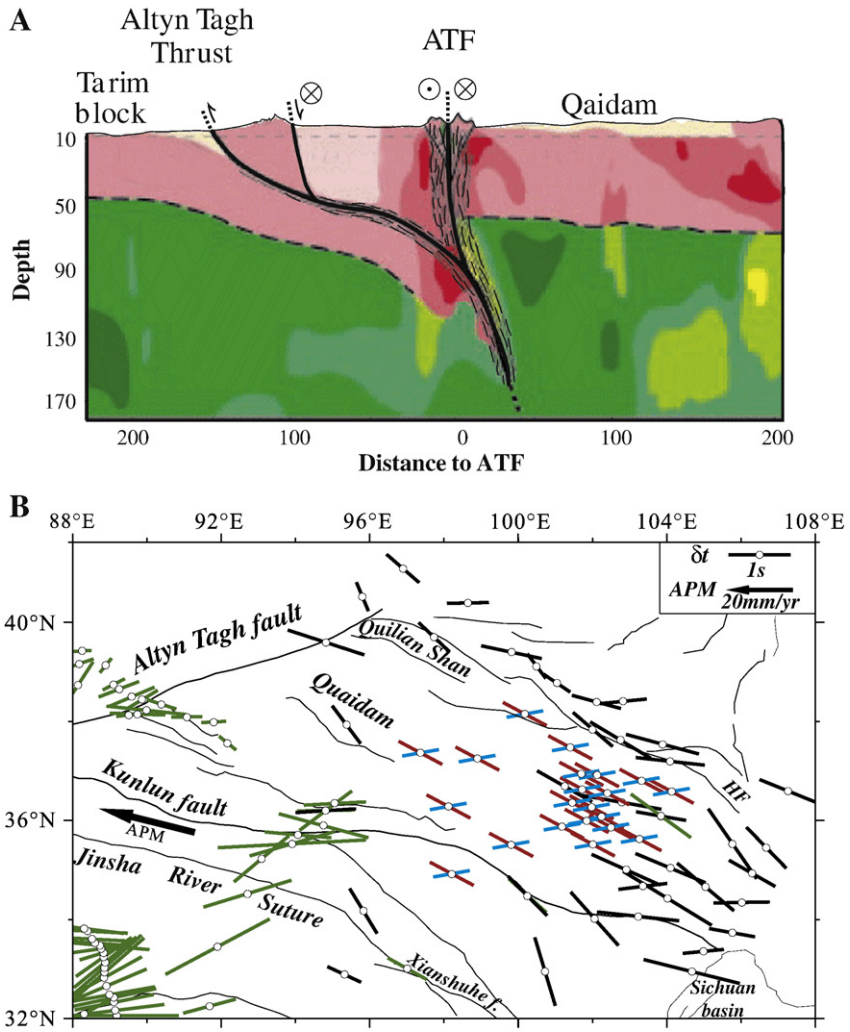

Fig. 14. Mantle deformation in the Himalayas. (A) Interpretative cross-section across the Altyn Tagh Fault system (Wittlinger et al., 1998) showing superimposed P-wave velocity structure and main geological structures. The P-wave velocity model reveals a low velocity anomaly below the fault down to 140 km. Red and green colors correspond to the crust and mantle, respectively. Darker colors in both layers indicate domains of higher P-wave velocities. (B) Shear wave splitting in Tibet (Li et al., 2011). Data recorded across the Altyn Tagh (Herquel et al., 1999) and Kunlun faults (Guilbert et al., 1996; McNamara et al., 1994) show that, approaching the fault zone, the polarization of the fast S-wave rotates to parallelism with the fault zone, suggesting that these faults penetrate deep into the lithospheric mantle. Data in eastern Tibet from Li et al. (2011) show a consistent pattern with either a single-layer or a two-layer structure (blue bars = upper layer, interpreted as the crust by Li et al., 2011; red bars = lower layer, interpreted as the lithospheric mantle) suggesting that the fabric in the lithospheric mantle is parallel to the fault system.

In stable continental lithosphere, shear wave splitting measurements in the vicinity of major fossil strike-slip faults suggest that fault-related olivine CPO may be frozen in the lithospheric mantle for hundreds of millions of years. Recently, Bastow et al. (2007) used a dense seismological network (~20 km spacing between stations) to map the seismic anisotropy in the vicinity of three major Caledonian fault zones in the Scottish Highlands: the Highlands Boundary Fault, the Great Glen transcurrent fault and the Moine Thrust. This experiment revealed two domains displaying contrasted seismic anisotropy patterns (Fig. 15). North of the Moine Thrust, ENE to NE fast S-wave polarizations and moderate delay times were consistently observed. South-eastward, approaching the Great Glen Fault, the fast S-wave polarization progressively rotates into parallelism with the fault trend and the delay time increases significantly. NE fast polarizations, but lower delay times are observed between the Great Glen and the Highlands Boundary faults. Based on these observations, Bastow et al. (2007) conclude that: (1) the source of anisotropy is in the lithospheric mantle, (2) the coherence between the Moine Thrust kinematics and the fast S-wave polarization in the north-eastern domain supports an anisotropy due to a thrust fabric in the lithospheric mantle inherited from the Silurian activity of the fault, and (3) the change in polarization direction approaching the Great Glen Fault results from a strike-slip fabric in the lithospheric mantle beneath the surface expression of this fault, as previously proposed by Helffrich (1995) and Barruol et al. (1997a).

Another interesting example supporting crust–mantle coupling beneath major fossil strike-slip faults comes from the Superior Province of North America. Shear-wave splitting measurements in the vicinity of the Great Slave Lake Shear Zone (GSLSZ), a paleoproterozoic dextral transcurrent fault several tens of kilometers wide, show a polarization of the fast split S-wave consistently parallel to the trace of the fault over a region ~150 km wide (Sénéchal et al., 1996). Long period magnetotelluric soundings have shown that the electrical conductivity in the lithospheric mantle is also faster along the strike of the GSLSZ, that is, subparallel to the polarization of the fast S-wave (Mareschal et al., 1995). This electrical conductivity anisotropy was interpreted as due to preferential alignment of graphite films along grain boundaries (Mareschal et al., 1995) and the slight obliquity between fast seismic and electrical directions proposed as a shear sense indicator (Ji et al., 1996). The physical causes behind the anisotropy of electrical conductivity in the mantle are still controversial (preferential orientation of graphite or melt films along grain boundaries, anisotropic diffusion of H+ and olivine CPO…). Yet the good correlation between seismic and

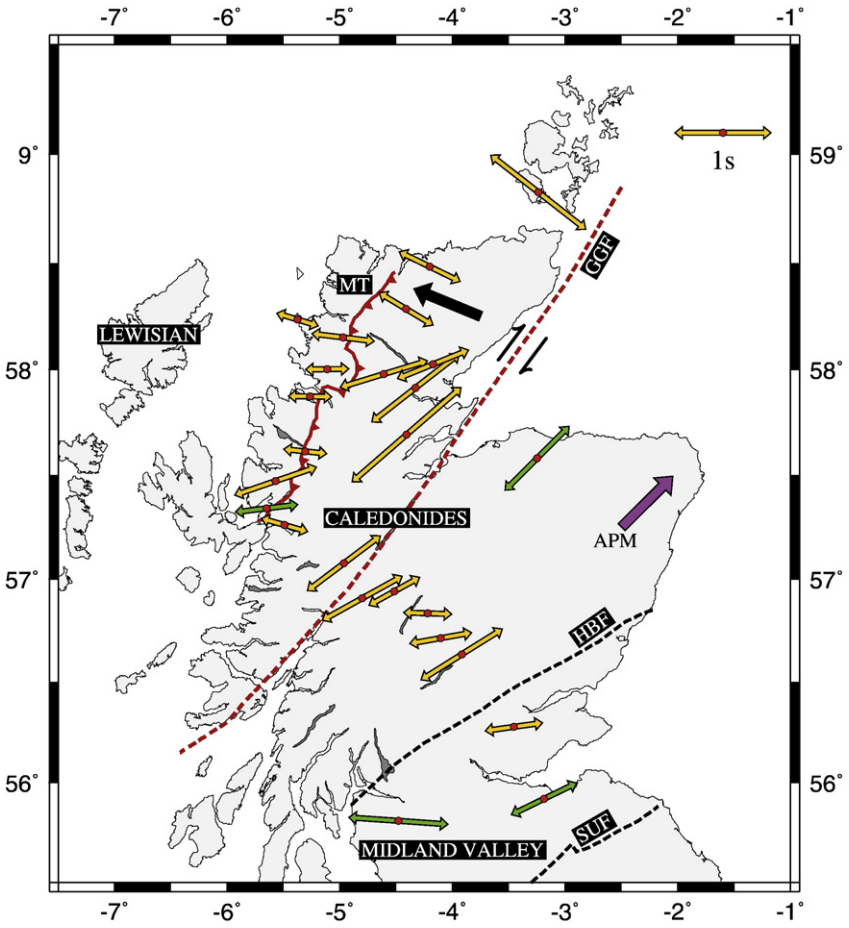

Fig. 15. Shear wave splitting in the Scottish Highlands. This figure shows the direction of the fast split S-wave polarization in the dense RUSH seismological network (yellow arrows (Bastow et al., 2007)) and previous data (green arrows) from Helffrich (1995). From the Moine Thrust (MT) to the Great Glen Fault (GGF), a rotation of the fast S-wave polarization and an increase in delay time are clearly visible. HBF: Highlands Boundary Fault; SUF: Southern Uplands Fault; APM: absolute plate motion. The black arrow shows the direction of thrusting along the Moine Thrust during the Silurian.

electrical anisotropies and the strike of the GSLSZ supports that deformation associated with this fault produced a coherent fabric (CPO and preferred orientation of grain boundaries) in the lithospheric mantle at scales $\geq$100 km.

Geophysical observations provide evidence of seismic anisotropy indicating strike-slip deformation in the lithospheric mantle beneath most major transcurrent faults, but a few counter-examples also exist. The most puzzling is probably the North Anatolian Fault, which accommodates, at the surface, most of the displacement of the Anatolia microplate relative to central Europe (Fig. 1). Shear-wave splitting measurements performed across the fault show fast polarizations consistently NE–SW, at large angle to the trace of the fault (Fig. 16), which are interpreted as due to southwestward asthenospheric flow, possibly related with retreat of the Alpine subduction zones (Biryol et al., 2010; Sandvol et al., 2003). No evidence of multiple anisotropy layers has been observed. Absence of shear-wave splitting related to the fault may be interpreted as due to: (1) a width of the shear zone smaller than the Fresnel zone of teleseismic shear-waves in the lithospheric mantle (~50 km), or (2) a destructive summation of the lithospheric and asthenospheric anisotropies beneath the fault. The lack of good back-azimuthal coverage in the data does not allow discriminating between these two interpretations.

In summary, seismological techniques provide key observations supporting the continuation of major faults/shear zones into the lithospheric mantle. Seismic reflection profiling detects gently to moderately dipping reflectors in the mantle that are usually interpreted as the continuation at depth of normal faults and, more rarely, thrust faults. Yet vertical faults or shear zones may only be imaged by these techniques when there is a clear contrast in seismic wave velocity between the domains bounded by the fault, or when they are associated with Moho offsets. In this latter case, the shear zone accommodates a vertical component of deformation that may be due to transtensional or transpressional deformation, or, to reactivation as normal faults. Another limitation from imaging faults or shear zones in the mantle by seismic profiling and of receiver function analysis is that to be a reflector, a fault zone has to be associated with a contrast in acoustic impedance, which is the product of seismic wave velocity and density. This requires a significant variation of the mantle mineralogy, the presence of fluids or of substantial amounts of hydrated minerals in the fault zone, or a contrast in seismic anisotropy between the fault zone and the surrounding mantle. The last process is likely, since shearing results in reorientation of the olivine CPO relatively to the surrounding medium. Strain localization may result either in a stronger or a weaker crystallographic preferred orientation in the shear zone depending on the temperature conditions under which deformation occurs and on the strain magnitude. Natural examples consistently show that grain-size reduction during mylonitization is accompanied by a weakening of the CPO (*e.g.*, Falus et al., 2011; Kaczmarek and Tommasi, 2011; Warren and Hirth, 2006). Reflectors formed in a relatively cold mantle (<900 °C) might thus represent shear zones composed of fine-grained mylonites having a weaker CPO compared to the surrounding mantle. However, several seismological observations suggest a rather large anisotropy associated to mantle reflectors (*e.g.*, Bostock, 1999), which implies strong olivine CPO in the fault zone. Hence, these anisotropic reflectors probably do not represent fine-grained mylonitic zones in the mantle.

Fig. 16. Shear wave splitting across the North Anatolian Fault (Biryol et al., 2010; Sandvol et al., 2003; image from Google Earth - TerraMetricsCNES/Spot Image - Digital Globe 2011). Polarization of the fast split S-wave (white arrows) is consistently NE-trending, showing no correlation with the trace of the fault (in red, from Şengör et al., 2005). Stars at stations indicate apparent isotropy ("null" anisotropy measurements).

Shear wave splitting measurements may only detect rather large anisotropic domains (both vertically and laterally). In most cases, low-angle faults, either normal or reverse, do not generate splitting large enough because the wave path in the anisotropic shear zone is too short. Increasing localization and decreasing CPO under decreasing temperature conditions, as observed in peridotite massifs, would further decrease the probability to detect low-angle faults with shear wave splitting. On the other hand, for vertical strike-slip faults, a teleseismic S-wave can travel a long distance in the fault zone. A major strike-slip fault crosscutting the entire lithospheric mantle should thus generate large S-wave splitting, provided its width is comparable to the wavelength of the incoming S-wave. This explains why clear fault-related anisotropy signals are observed beneath most major intra-continental strike-slip faults and transform boundaries.

5. Shear zones width and the rheology of the lithospheric mantle

The association of geological and geophysical data highlights a large range of strain localization processes and shear zone widths in the lithospheric mantle. Observations in peridotite massifs and ophiolites show that mylonitic zones hundreds of meters to a few km wide may form in the lithospheric mantle in response to deformation under retrograde pressure–temperature conditions or in the presence of melt or fluids. These km-scale shear zones, characterized by sharp limits, may explain mantle reflectors observed by refraction data in the shallow lithospheric mantle. Peridotite massifs are, however, mostly composed of coarse-grained peridotites with pervasive foliations and lineations, low-stress microstructures, and well-developed olivine crystal preferred orientations suggesting that, under high-temperature conditions, localization takes place at scales larger than the massifs exposure extent. Seismic anisotropy data suggest that, in the lithospheric mantle below major strike-slip faults, strain localizes in shear zones at least tens of km wide. Although these observations are indirect or limited by the size of exposures, they point to an inverse relation between shear zone width and strength. This relation is similar to the one observed in the crust (Fig. 3), where fault/shear zone width increases with depth (and thus with temperature) from cm to meters close to the surface to several tens of kilometers in the middle to lower crust of hot orogens.

Temperature has a major effect on localization of strain because it controls the rock strength. In a recent article, Platt and Behr (2011) have proposed that ductile/viscoplastic deformation in lithospheric-scale shear zones occurs at approximately constant stress conditions corresponding to the yield stress of the undeformed surrounding rocks under the pressure and temperature conditions prevailing at the considered depth. This simple approach is appealing; it is consistent with observations indicating that the width of shear zones tends to be inversely proportional to the rock strength, and thus proportional to temperature. It is also consistent with the progressive strain localization that characterizes retrogressive shear zones. However, experiments show that the yield stress of a rock depends on the imposed strain rate, which in turn depends on the width over which strain is distributed; the solution obtained with this constant stress approach is therefore non-unique.

An alternative approach would be to consider that the 'ideal' strain distribution should minimize the total mechanical work of the system through an optimization of the microstructure and deformation mechanisms. When temperature decreases, as during exhumation, the rock strength increases. An intuitive reasoning, in agreement with observations in natural shear zones, would imply that as the rock strength increases, the total available energy in the system allows deforming increasingly smaller volumes, leading to progressive strain localization. Within the active shear zone the work rate by unit volume will be higher (deviatoric stress and strain rate are higher) and, because the equilibrium grain size is inversely proportional to the rate of mechanical work (Austin and Evans, 2007), grain-size reduction occurs. Yet, a simple calculation shows that in the absence of intrinsic weakening processes the total work rate of a system submitted to shearing is minimized by distributing the deformation over the largest possible volume. The strain weakening processes should thus precede strain localization and not be a consequence from it.

5.1. How is strain localization seeded?

Strain localization may be triggered by: (i) "external" processes, related to the boundary conditions, (ii) inherited features, such as heterogeneity and anisotropy, or (iii) intrinsic material (rock) properties and/or their modification under applied stress (*e.g.*, Montési and Zuber, 2002; Paterson, 2007).

5.1.1. Interactions with brittle faults

Strain localization in the downward extension of a brittle fault is imposed by boundary conditions (*e.g.*, Paterson, 2007). Numerical models show that stress transfer from the lower tip of a frictional fault results in enhanced strain rates in a lobe extending down dip into the ductile layer; strain rates are maximum just below the tip of the frictional fault and decay with increasing depth and time (Ellis and Stockhert, 2004). The magnitude of the strain enhancement and the actual geometry of the strain localization lobe depend on the rheology of the ductile layers; thermal weakening in the vicinity of the fault results in effective strain rate enhancement (by a factor 50) up to the middle crust. Extension of this interaction into the lithospheric mantle was not constrained by these models, which focused on crustal deformation, but the fast decrease of the stress perturbation with increasing distance from the frictional fault tip suggests that this effect is minor. Such interactions are however invoked for explaining post-seismic deformation associated with major earthquakes in California, Alaska, or Iceland (*e.g.*, Árnadóttir et al., 2005; Freed et al., 2012; Pollitz, 2005; Pollitz et al., 2001). The implications of these data for rheology of the lithospheric mantle are discussed in the next section.

5.1.2. Inherited rheological heterogeneities

Rheological heterogeneities (pre-existing domains with contrasting strength) may account for strain localization from the mm-scale, as in rocks composed by two or more minerals with contrasted strengths (*e.g.*, Barnhoorn et al., 2005), to the plate tectonic scale, where lateral variations of the geotherm result in strength contrasts within a plate (*e.g.*, Neves et al., 2008; Tommasi et al., 1995; Vilotte et al., 1984). Both weak and strong domains induce strain localization. Stiff heterogeneities, such as hard crystals in a rock or a cratonic domain in a continental plate, generate local stress concentrations and strain localization at their tips. If multiple heterogeneities are present, strain transfer between the various heterogeneities leads to development of continental-scale shear zones (*e.g.*, Tommasi et al., 1995; Vauchez et al., 1998).

Rheological heterogeneities may also form during deformation due, for instance, to injection of melt or fluids into the deforming system. Magmas and fluids, even in small proportion, result in strong weakening of both mantle and crustal rocks. Increasing melt fraction and water content result in strong weakening in olivine-rich rocks (Hirth and Kohlstedt, 2003; Zimmerman and Kohlstedt, 2004). Development or not of strain localization depends however on the distribution of the fluids. If they are concentrated in a rather small volume compared to the size of the system, magmas and fluids may trigger strain localization. On the other hand, if melt or fluids are homogeneously distributed through the entire system, they may favor homogeneous strain repartition because the effect on rock strength is so large that it tends to erase any pre-existing heterogeneity (*e.g.*, Vauchez et al., 2007). Analysis of the deformation distribution in fossil lithosphere–asthenosphere boundaries exposed in the Lanzo, Lherz, and Ronda peridotite massifs (Kaczmarek and Tommasi, 2011; Le Roux et al., 2008; Soustelle et al., 2009) or in the mantle section of ophiolites (*e.g.*, Allerton and Macleod, 1998; Boudier and Coleman, 1981; Kelemen and Dick, 1995) clearly points for strain localization in melt-rich domains, implying a feedback between melt or fluids transport and deformation. These observations lead to a chicken-or-egg dilemma: is the deformation localized by the presence of melt or does the deformation favor melt focusing? Simple shear experiments in olivine + MORB composites show melt segregation into bands at low angle to the shear plane, which localize strain (Holtzman et al., 2003; King et al., 2010). Evidence for melt segregation is less evident in natural systems, but this process has been proposed to explain the pervasive, mm-scale websteritic layering in the lherzolites in Lherz (Le Roux et al., 2008) or the layered structure of the Moho transition zone in the Oman ophiolite (Higgie and Tommasi, submitted). There is however a major difference between experiments and nature: in experiments melt-rich bands are oblique (~20°) to the shear plane and their orientation is controlled by the stress field (Holtzman et al., 2003), while in nature they are parallel to the foliation. Zimmerman et al. (1999) have suggested that this difference is due to the relaxation of the stress field in the nature.

5.1.3. Inherited structural heterogeneity

Structural heterogeneity occurs when the deforming system involves domains with variable fabric that may generate a mechanical anisotropy. Olivine, because it has only 3 independent slip systems, displays a highly anisotropic mechanical behavior during ductile deformation by dislocation creep. At high temperature and moderate pressure, an olivine crystal deforms up to 100 times faster if oriented as to activate the 'easy' (010)[100] slip system rather than the 'hard' (010)[001] system (Bai et al., 1991; Durham and Goetze, 1977). This viscoplastic anisotropy is responsible for the development of strong CPO during deformation of mantle rocks by dislocation creep. Similarly to the elastic anisotropy, part of this viscoplastic anisotropy is transferred to the rock and lithospheric scales *via* the CPO of olivine. As a consequence, the strength of the upper mantle varies as a function of the orientation of the applied stress relative to the olivine CPO. This behavior may be expressed macroscopically as an anisotropic viscosity.

Seismic anisotropy measurements support the existence of frozen olivine CPO with orientations coherent at the scale of several tens of km in the lithospheric mantle; its viscosity should therefore be anisotropic. Based on these premises and on the observation of tectonic fabric reactivation during continent break-up, Vauchez et al. (1997) proposed that reactivation at the "plate tectonic-scale" is favored by the mechanical anisotropy of the lithospheric mantle, which is due to the olivine CPO developed during past tectonic events. Polycrystal plasticity models confirmed that a pre-existing olivine CPO induces an anisotropic mechanical behavior of the lithospheric mantle (Tommasi and Vauchez, 2001). These results were corroborated by recent multiscale 3D models that explicitly consider an evolving CPO-controlled viscoplastic anisotropy (Knoll et al., 2009; Tommasi et al., 2009). Lateral variations in the orientation and intensity of the pre-existing olivine CPO within a plate result in strain localization; domains in which the orientation of pre-existing olivine CPO allows high resolved shear stresses on the 'easy' (010)[100] and (001)[100] slip systems for most crystals deform faster (Tommasi et al., 2009). This condition is met, for instance, when the boundary conditions impose shearing parallel to the pre-existing foliation and lineation in the mantle (Fig. 17), even if the shear sense is inverted (Bauschinger effect; Bruijn et al., 2011; Delle Piane and Burlini, 2008). Low strengths are also observed in domains submitted to extension or compression oblique to the pre-existing tectonic fabric (Tommasi et al., 2009). These models also highlight that the deformation of an anisotropic viscoplastic mantle, where the olivine CPO controls anisotropy, has a characteristic signature: a shearing component of deformation parallel to the pre-existing mantle fabric.

5.1.4. Strain localization due to changes in rock-properties or physical conditions

Strain localization may also arise from rheological heterogeneities produced by the deformation. The main sources for intrinsic localization are: (i) thermo-mechanical coupling (shear heating), (ii) modification the rock fabric (microstructure or CPO), or (iii) reaction-induced

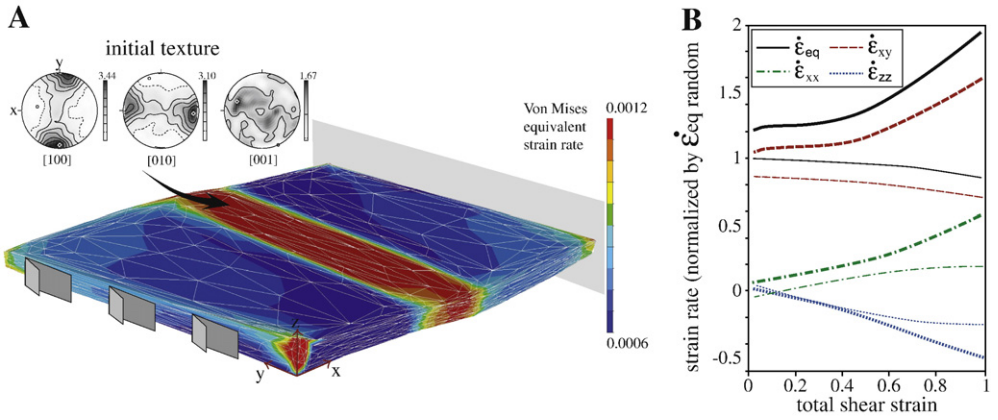

Fig. 17. (A) Geometry, boundary conditions, and Von Mises equivalent strain rate $\dot{\varepsilon}_{eq} = \sqrt{2/3}\dot{\varepsilon}_{ij}\dot{\varepsilon}_{ij}$ distribution in a model in which strike-slip motion is imposed parallel to an 'inherited transcurrent shear zone' after a total shear strain of 0.75. Texture-induced anisotropy results in progressive strain localization in the 'inherited shear zone' that deforms up to 2 times faster than the surroundings that had an initially random olivine crystal preferred orientation. Upper left inset displays the initial olivine texture in the 'inherited shear zone'. (B) Evolution of the strain rate (normalized by the Von Mises equivalent strain rate $\dot{\varepsilon}_{eq}$ in a medium with a random texture submitted to the same boundary conditions, *i.e.*, the initial equivalent strain rate in the surrounding medium) as a function of the total shear strain. Thick and thin lines in (B) indicate strain rates in the inherited shear zone and in the surrounding medium, respectively. Evolution of the olivine crystal preferred orientations with increasing strain results in further strain localization in the 'inherited shear zone'. Extension normal to the shear zone and thinning arise due to a slight obliquity of the olivine crystal preferred orientations relative to the fault trend.

weakening. A large amount of theoretical work has been devoted to shear heating (*e.g.*, Fleitout and Froidevaux, 1980; Lu et al., 2011; Regenauer-Lieb and Yuen, 2004) showing that it may be effective in high strain rate/high stress domains, but clear evidence for it in natural ductile shear zones is still missing. In the following, we will focus on the other two processes, which have been proposed to play an important role in the Earth's upper mantle based on observations of naturally deformed peridotites and laboratory experiments.

The rock fabric (grain size and shape distributions) evolves in response to the competing effects of deformation, recovery, recrystallization, and grain growth. A widely-accepted model, based on extrapolation of flow laws derived from high-temperature, high-stress experimental data, proposes that grain-size reduction by dynamic recrystallization promotes a transition in dominant deformation mechanism from dislocation creep to a grain-size sensitive creep, where grain boundary sliding is assisted by diffusion (*e.g.*, Hirth and Kohlstedt, 2003). In this regime, grain size reduction produces strain-weakening and may consequently lead to strain localization. Large shear experiments on calcite and olivine polycrystals show strain softening associated with grain-size refinement by dynamic recrystallization and development of strong crystal preferred orientations (Barnhoorn et al., 2004; Bystricky et al., 2000; Pieri et al., 2001a, 2001b). However, despite a large grain size reduction, these experiments do not show strain localization or evidence for a transition from dislocation creep to grain-size sensitive creep: crystal preferred orientations are well developed and stress exponents are ≥ 3. As reviewed in previous sections, microstructures and olivine CPO in naturally deformed peridotites point to a similar conclusion: grain-size reduction by dynamic recrystallization does not result in a change in dominant deformation mechanism. Evidence for grain-boundary sliding in naturally deformed peridotites is restricted to mm-scale ultramylonite bands in which extreme grain-size refinement is favored by reactions.

In polyphase rocks composed by minerals with contrasting strengths, deformation may trigger phase segregation, forming mono-mineralic layers parallel to the shear plane or foliation. This structural evolution results in a mechanical anisotropy (the shear viscosity parallel to the layering is reduced) and allows more efficient laminar flow. Segregation and strain localization in the weak-phase layers are observed at high strains in torsion experiments on two-phase solid aggregates with a strong rheological contrast, such as calcite and quartz (Rybacki et al., 2003) and anhydrite and calcite (Barnhoorn et al., 2005). Strain localization associated with phase segregation was also observed in experiments on quartz–plagioclase–biotite aggregates (Holyoke and Tullis, 2006). These experiments suggest that strain localization in a two-phase aggregate with a strong rheological contrast depends on a connectivity threshold for the weak phase that is reached under the action of progressive deformation. This threshold and the rheological contrast required to produce strain localization are however difficult to quantify, since they depend on the initial arrangement of the weakest phase. Compositional layering, characterized by variations in the relative proportion of olivine and pyroxenes, is a common feature of mantle rocks. The rheological contrast between olivine and pyroxenes is indicated by the common boudinage of pyroxenite layers. However, as olivine is both the weakest and the dominant phase, this compositional layering may induce anisotropy, but not significant weakening.

Another effect of deformation, already presented in the previous section, is the development of strong crystallographic preferred orientations that generate a mechanical anisotropy. The importance of mechanical softening associated with the progressive development of a CPO is corroborated by the onset of weakening in torsion experiments at low shear strains ($\gamma = 0.07$ and 1 for olivine and calcite, respectively), when the fraction of recrystallized grains is still small (Barnhoorn et al., 2004; Bystricky et al., 2000), as well as by the permanent softening observed in forward and reverse torsion experiments in calcite (Bruijn et al., 2011). Another observation pointing to the effect of CPO evolution on the mechanical behavior is the difference in stress–strain curves for simple shear and axial compression or extension experiments. Although dynamic recrystallization and grain-size reduction occurs in both types of experiments, strain softening is only commonly observed in simple shear. The exception is the experimental extension of marble performed by Rutter (1998, 1999), which showed strain softening associated with recrystallization at extensional strains of *ca.* 1000%. In traditional axial compression experiments to 20% strain, peak stress is followed by a steady-state behavior (*e.g.*, Chopra and Paterson, 1981). In summary, evolution of the CPO during simple shear to high strain produces weakening and may thus lead to strain localization. However almost all experiments in torsion have been done in a constant shear strain-rate and no localization has been observed in single-phase aggregates. Based on this observation, Paterson (2007) undertook a new theoretical study of the cause of localization in torsion experiments; his analysis predicted that localization should occur in olivine aggregates at constant stress (torque), but not

at constant strain-rate. Recent experiments by Hansen et al. (2012) have confirmed the predictions of Paterson, especially that boundary conditions play an important role in localization.

Reaction-induced softening may result from crystallization of weaker mineral phases and/or from the grain refinement associated with the nucleation process (*e.g.* Rutter and Brodie, 1988). Strain localization associated with hydration reactions has, for instance, been described in the Erro-Tobio massif in the Southern Alps and Lizard ophiolite (Allerton and Macleod, 1998; Vissers et al., 1991). Reactions associated with the transformation of a spinel-lherzolite assemblage into a plagioclase-lherzolite have also been proposed to explain strain localization and formation of ultramylonite bands in various peridotite massifs, such as Turon de la Técouère, Hidaka, and Lanzo peridotite massifs (Furusho and Kanagawa, 1999; Kaczmarek and Tommasi, 2011; Newman et al., 1999). In these examples, reaction products form ultrafine aggregates, which polymineralic nature hinders grain growth, allowing for activation of grain boundary sliding, as evidenced by observation of planar grain boundaries parallel to the foliation and very weak, almost random crystal preferred orientations. Recent studies highlight, however, that pre-existing grain size refinement is essential to the onset of these retrograde reactions (Newman and Drury, 2010). Laboratory data suggests that the reaction kinetics may be enhanced by non-hydrostatic stress (*e.g.*, Demouchy et al., 2011; Keller et al., 2010), suggesting a further possible positive feedback between reaction and deformation. Finally, exothermic reactions, such as the hydration of olivine to form serpentine, may also contribute to softening through the heat release.

5.2. Constraints on the lithospheric mantle rheology beneath major faults

Analysis of the post-seismic velocity field following major earthquakes was proposed to provide *in situ* data on the lithospheric mantle rheology beneath major faults. These studies are based on the hypothesis that the sudden increase in differential stress associated with a large magnitude earthquake results in faster viscous flow in the lower crust and uppermost mantle, which transfers stress back into the elasto-plastic upper crust. Fitting of the post-seismic crustal deformation field allows therefore estimating lower crust and mantle viscosities (*e.g.*, Pollitz, 2005; Pollitz et al., 2001). All recent models converge on the following points: (i) lower crust viscosities almost one order of magnitude higher than upper mantle ones, (ii) low long-term mantle viscosities ($<10^{20}$ Pa.s), and (iii) a weaker transient viscous behavior characterized by viscosities initially ten times lower than the long-term ones are necessary to explain the magnitudes and time-decay of post-seismic velocities (*e.g.*, Freed et al., 2012; Pollitz and Thatcher, 2010). Pollitz and Thatcher (2010) also argued, based on a formal resolution analysis, that post-seismic velocity data has the power to resolve vertical variations in the long-term mantle viscosity for depths ≤ 60 km. They show that post-seismic deformation following the 1999 Hector Mine earthquake in southern California is better fit by models with a weak increase in viscosity with depth, and that introduction of a strong lid (a factor 10 increase in viscosity in a 10 km layer just below the Moho) significantly decreases the fit to the data.

Long-term strengths of the uppermost lithospheric mantle derived from post-seismic data imply therefore in a weak lithospheric mantle beneath lithospheric-scale faults. Several mechanisms have been proposed to account for these low viscosities, like hydration of the lithospheric mantle or small grain sizes allowing deformation by diffusion creep (Freed et al., 2010; Pollitz and Thatcher, 2010). The data on peridotite massifs reviewed in the previous sections argues, however, against softening by activation of grain-size sensitive creep over large volumes in the lithospheric mantle. Consistently, recent forward models indicate that the post-seismic deformation following the Hector Mine earthquake in eastern California is best fit by models that consider a very hot geotherm (1200–1330 °C at 50 km depth) and a wet mantle (1000 H/Si[6], that is ~60 ppm wt) deforming by dislocation creep (Freed et al., 2012). These high water contents in olivine are, however, not consistent with data from spinel-bearing xenoliths, which systematically show <20 ppm wt H_2O, even after correction for hydrogen loss during extraction (Demouchy et al., 2006; Peslier, 2010). Moreover, the water solubility in olivine decreases strongly with decreasing temperature; it varies from >500 ppm wt at 1200 °C/2.1 GPa to ~35 ppm at 900 °C/1.5 GPa and only 16 ppm wt H_2O at 700 °C/1 GPa (Zhao et al., 2004). Water incorporation in olivine cannot therefore significantly reduce the strength in the cold uppermost lithospheric mantle.

A very hot geotherm may account for low strength in the lithospheric mantle even if water contents in olivine are ≤ 20 ppm wt as those observed in spinel-bearing peridotite xenoliths. For instance, the long-term strain rates of 3×10^{-15} s^{-1} inferred for eastern California result in stresses in the lithospheric mantle <16 MPa if temperatures at the Moho are >800 °C. Note that the several tens of km wide shear zone beneath the San Andreas Fault inferred from seismic anisotropy data are consistent with low strength in the lithospheric mantle beneath California. Hot geotherms are also inferred for other areas displaying clear post-seismic deformation, like Alaska, Iceland, and the Andes (Árnadóttir et al., 2005; Khazaradze et al., 2002; Pollitz, 2005).

No long wavelength post-seismic deformation was, on the other hand, observed after the 2006 M_w7.0 Mozambique (Machaze) normal-faulting earthquake, which affected a 100 km thick lithosphere with a normal geotherm, suggesting viscosities greater than 2×10^{19} Pa.s in the ductile lithosphere beneath the fault (Copley et al., 2012). This observation highlights that this technique is unable to resolve the rheology of the lithospheric mantle in a non-thinned continental plate.

The actual strength of the shallow lithospheric mantle, in particular in continental domains with normal to cold geotherms remains a major question in geodynamics. Extrapolation of empirical flow laws derived from high-temperature and high strain rate experiments implies high strength in the shallow lithospheric mantle of a 100 km thick plate (>500MPa; Chopra and Paterson, 1981, 1984; Hirth and Kohlstedt, 2003). However, this extrapolation is based on the assumption that the parameters in these flow laws: apparent activation energy and volume as well as the pre-exponential parameter, are constant, depending on neither deviatoric stress nor temperature. This strong hypothesis cannot be tested, since the temperature/stress ranges on which experiments can be performed are limited. Experimental work in progress on the deformation of olivine single crystals between 800 °C and 1100 °C will probably shed a new light on the deformation of olivine under low temperature conditions. Preliminary experiments, during which olivine crystals oriented to activate slip on the (001)[100] and (100)[001] slip systems were deformed between 900 °C and 1200 °C, suggest that extrapolation of flow laws derived from high-temperature laboratory experiments largely results in a strong overestimation of the mantle strength for temperatures below 1000 °C (Demouchy et al., 2009). Yield stresses in these experiments are even lower than those predicted by using the low-temperature creep (exponential) flow law of Evans and Goetze (1979).

6. Summary and conclusions

Field observations in continental and oceanic peridotite massifs, mantle xenolith studies, seismic reflection profiling, receiver function analysis, seismic anisotropy measurements, and magnetotelluric soundings consistently support that strain localization does occur in the lithospheric mantle. Seismic reflection profiles and seismic anisotropy measurements suggest that mantle faults are usually connected to major crustal faults. A continuity of major crustal faults in the uppermost mantle is also in agreement with conclusions drawn from the analysis of post-seismic deformation in several active areas. Geological, geophysical and geochemical data converge therefore toward a model of lithospheric-scale faults along which the brittle crust, the ductile crust, and the lithospheric mantle are, on the long term, deformed coherently.

Observations are however different for faults that accommodate essentially vertical displacements (extensional shear zones or thrusts) and for strike-slip faults. Seismic anisotropy data support coherent deformation of the crust and the mantle beneath major strike-slip faults and transform plate boundaries, with shearing in the mantle distributed over domains a few tens to more than 100 km wide. High delay times ($\geq$1 s) between the fast and slow S-wave arrivals require a deformation of the entire lithospheric mantle. Moreover, high Pn anisotropy beneath these faults suggests strong olivine CPO even in the uppermost lithospheric mantle. This observation is in contrast with dispersion of the olivine CPO observed in most fine-grained mylonitic peridotites resulting from dynamic recrystallization under decreasing PT conditions. It is, though, consistent with the low-stress microstructures and strong olivine CPO observed in mantle xenoliths sampling the shallow mantle beneath the San Andreas Fault. Yet, seismic data do not allow ruling out the presence of mm-scale ultramylonitic bands in the shallow lithospheric mantle, since they affect too small volumes to be detected by seismic measurements. Electric measurements might have the potential to detect fine-grained mylonite zones in the uppermost mantle. Laboratory measurements support that fine-grained peridotites may display electrical conductivities up to 2 orders of magnitude higher than coarser-grained samples (ten Grotenhuis et al., 2004). Interpretation of high conductivity zones detected in the uppermost mantle beneath faults is however non-univocal since several parameters, such as fluids or other conductive phases along grain boundaries, may increase the conductivity of mantle rocks.

Penetration of thrust faults in the mantle is less clear. It is suggested by Moho offsets, interpreted as mantle slivers in the Alps and Pyrenees for instance, as well as by rare observations of shallow mantle reflectors beneath orogenic belts. Moreover, S-wave splitting data in thrust-dominated domains of convergence zones rarely show polarization of the fast S-wave consistent with thrusting in the mantle. One notable exception is the Moine Thrust (Bastow et al., 2007). Two interpretations are possible: (i) convergence is accommodated by different kinematics in the lithospheric mantle or (ii) thrust zones are too thin and ill-oriented (at high angle to the ray paths) to produce significant splitting. Predominance of belt-parallel fast S-wave polarizations in many orogenic belts (Barruol et al., 1997a, 1997b; Vauchez and Nicolas, 1991) favors nevertheless the first hypothesis, suggesting that the lithospheric mantle in many convergent plate boundaries undergoes homogeneous transpressional deformation, in contrast with crustal deformation that is often partitioned between orogen-parallel and orogen-normal tectonic motions. Finally, receiver function analysis has detected a large number of reflectors in the deep lithospheric mantle in cratonic domains. The interpretation of these reflectors in terms of mantle structure and dynamics is however still poorly constrained.

Extensional shear zones penetrating up to 10 km in the lithospheric mantle are inferred from seismic profiles showing subcrustal seismic reflectors and Moho offsets. Extensional shear zones <100 m to 1–2 km wide are also observed in peridotite massifs. Thermobarometric data and analysis of the microstructures of these sheared peridotites suggest that progressive strain localization occurred under decreasing pressure and temperature conditions, probably due to progressive exhumation of the footwall (Fig. 3). This results in an asymmetry of the shear zone from high temperature mylonites in the footwall to low temperature ones in the hanging wall. Increasing dynamic recrystallization results in a decrease in strength of olivine crystal preferred orientations from the footwall to the hanging wall. The resulting contrast in intrinsic anisotropy across the shear zone may generate seismic impedance, but whether the latter is large enough to explain the recorded seismic reflections or if the presence of fluids or serpentinization is also required remains an open question.

The review of the geophysical data highlights that mapping zones of localized deformation in the mantle is a difficult task. Seismic reflections in the mantle are rare, not easy to interpret, frequently discontinuous, and the technique is time consuming. The detection of variations in seismic anisotropy associated to possible mantle faults, although it has a good potential, lacks vertical resolution. Moreover, shear wave splitting measurements are not efficient for detecting low-angle, normal or reverse faults. Receiver function analysis allows the detection of reflectors in the lithospheric mantle, but the interpretation of these reflectors is still uncertain.

One major issue when studying strain localization in the mantle is the scale at which observations are performed compared to the scale at which fault-related deformation occurs. This raises the question of how representative is the evidence of strain localization found in peridotite massifs and even more in mantle xenoliths. In most orogenic peridotite massifs, the size of the initial zone of strain localization is larger than the massif itself and the most obvious evidence for strain localization is mylonitic to ultra-mylonitic shear zones that probably formed during exhumation of these massifs, as indicated by the decrease in shear zone width (and in recrystallized grain size) that points to deformation under retrogressive conditions. The rather abrupt variations in polarization direction of the fast split S-wave in the vicinity of some transcurrent faults support nevertheless that strain localization occurs, but at scales larger ($\geq$50 km) than the peridotite exposures at the Earth's surface. Shear zones several tens of km wide in the lithospheric mantle are in good agreement with the observed width of strike-slip faults in hot middle to lower felsic crusts, which may reach several tens of kilometers of localized deformation (Fig. 4). There is therefore a clear discrepancy between the scale of localization processes in the mantle and the scale of our direct observations. Mylonitic to ultramylonitic shear zones in the mantle likely represent adaptation of shear zone width to decreasing temperature conditions. They are probably not representative of the long-term, localized strain within steady-state fault zones, except perhaps in cold sub-Moho mantle.

Analysis and modeling of post-seismic velocity fields in the vicinity of major faults is a promising tool to unravel the rheology of the lithospheric mantle, but likely only applicable to low strength regions, generally characterized by hot geotherms. The rheology of the shallow lithospheric mantle and hence of strain localization beneath faults formed in a normal to cold lithosphere remains therefore an open question. The behavior of this layer represents, however, a crucial parameter to the crust–mantle mechanical interaction. Development of a viscosity anisotropy due to olivine crystal preferred orientations may entail lower strengths in the lithospheric mantle for both continued shearing across the fault/shear zone or its reactivation (Fig. 17). Although this CPO-induced mechanical anisotropy can only reduce the lithospheric mantle strength by a factor 5–6, it may play an essential role during the reactivation of large-scale lithospheric faults.

Reactivation of fault/shear zones is a major feature of continent deformation (*e.g.*, Holdsworth et al., 2001; Storti et al., 2003). Reactivation of brittle faults is frequently observed during basin inversion (*e.g.*, Salvini et al., 1997; Wilson et al., 2010). Butler et al. (2008) extended this model by suggesting that the structural fabric of crustal mylonites may also result in a directional weakening and hence guide the deformation in the continental crust. However these "crustal" processes cannot explain structural reactivation at the plate tectonic scale, such as repeated continental break-up along ancient collisional belts (Wilson, 1966) or the formation of linear arrays, hundreds of km long, of intraplate magmatism and seismicity (Sykes, 1978). An anisotropic viscosity of the lithospheric mantle due to olivine CPO frozen at the end of deformational events may account for most observations (Tommasi and Vauchez, 2001; Tommasi et al., 2009). The most efficient weakening occurs when the inherited tectonic fabric is reactivated by shearing in the same direction, even if the sense of shear is inverted (Fig. 17). This strongly favors systematic reactivation of major fault zones through geological times.

To conclude, the physics of strain localization in the ductile regime still remains poorly understood. A limited number of processes may

promote strain localization in the lithospheric mantle and some of these processes are only active locally. The most obvious and best-understood forcing factor is the coupling with brittle faulting in the upper crust. Melt-related strain localization is certainly effective at the lithosphere–asthenosphere boundary. Reaction-induced softening has been shown to produce strong strain localization in shear zones accommodating vertical displacements, where peridotites are submitted to varying pressure and temperature conditions. Only two processes may be active over the entire lithospheric mantle column: structural softening associated with recrystallization and geometrical softening due to development of crystal preferred orientations. Microstructures and CPO in naturally deformed peridotites consistently point to dominant deformation by dislocation creep, suggesting that even if recrystallization results in grain-size reduction, it does not lead to a change in dominant deformation mechanism to grain-size sensitive processes, like diffusion creep or grain boundary sliding. Besides the processes that trigger strain localization, how the width of the shear zones is regulated remains an open question. Observations support that the width of shear zones is inversely proportional to the strength of the sheared rocks, and thus to the work rate needed. There is yet no satisfactory law relating the shear zone width to physical parameters.

Acknowledgments

We are indebted to Fabrizio Storti and Timothy Horscroft who suggested writing this review paper. This was a good suggestion since we learned a lot working on the manuscript. We also realized that additional efforts are needed to better image and understand faults in the mantle and their coupling with crustal structures. We are grateful to two anonymous reviewers for their thorough discussion of the initial version of this review paper. Their constructive criticism and useful suggestions helped to improve several points of the manuscript. We are grateful to Françoise Boudier and Adolphe Nicolas who provided us pictures and information on the Oman ophiolite and to Sylvie Demouchy for kindly sharing the results of her on-going experiments on low-temperature deformation of mantle rocks.

Appendix A. Supplementary data

Supplementary data to this article can be found online at http://dx.doi.org/10.1016/j.tecto.2012.06.006.

References

Abramson, E.H., Brown, M., Slutsky, L.J., Zaug, J., 1997. The elastic constants of San Carlos olivine up to 17 GPa. Journal of Geophysical Research 102, 12,252–12,263.

Ai, Y., Zhao, D., Gao, X., Xu, W., 2005. The crust and upper mantle discontinuity structure beneath Alaska inferred from receiver functions. Physics of the Earth and Planetary Interiors 150, 339.

Allerton, S., Macleod, C.J., 1998. Fault-controlled magma transport through the mantle lithosphere at slow-spreading ridges. Geological Society of London, Special Publications 148, 29–42.

Alsina, D., Snieder, R., 1995. Small-scale sublithospheric continental mantle deformation: constraints from SKS splitting informations. Geophysical Journal International 123, 431–448.

Argus, D.F., Gordon, R.G., 2001. Present tectonic motion across the Coast Ranges and San Andreas Fault system in central California. Geological Society of America Bulletin 113, 1580–1592.

Árnadóttir, T., Jónsson, S., Pollitz, F.F., Jiang, W., Feigl, K.L., 2005. Postseismic deformation following the June 2000 earthquake sequence in the south Iceland seismic zone. Journal of Geophysical Research 110, B12308, http://dx.doi.org/10.1029/2005jb003701.

Assumpcao, M., Heintz, M., Vauchez, A., Silva, M.E., 2006. Upper mantle anisotropy in SE and Central Brazil from SKS splitting: evidence of asthenospheric flow around a cratonic keel. Earth and Planetary Science Letters 250, 224–240.

Austin, N.J., Evans, B., 2007. Paleowattmeters: A scaling relation for dynamically recrystallized grain size. Geology 35, 343–346.

BABEL Working Group, 1990. Evidence for early Proterozoic plate tectonics from seismic reflection profiles in the Baltic shield. Nature 348, 34–38.

Bai, Q., Kohlstedt, D.L., 1992. High-temperature creep of olivine single crystals. 2. Dislocation structures. Tectonophysics 206, 1–29.

Bai, Q., Mackwell, S.J., Kohlstedt, D.L., 1991. High-temperature creep of olivine single crystals. 1. Mechanical results for buffered samples. Journal of Geophysical Research 96, 2441–2463.

Barnhoorn, A., Bystricky, M., Burlini, L., Kunze, K., 2004. The role of recrystallisation on the deformation behaviour of calcite rocks: large strain torsion experiments on Carrara marble. Journal of Structural Geology 26, 885–903.

Barnhoorn, A., Bystricky, M., Kunze, K., Burlini, L., Burg, J.-P., 2005. Strain localisation in bimineralic rocks: experimental deformation of synthetic calcite–anhydrite aggregates. Earth and Planetary Science Letters 240, 748–763.

Barruol, G., Ismail, W.B., 2001. Upper mantle anisotropy beneath the African IRIS and Geoscope stations. Geophysical Journal International 146, 549–561.

Barruol, G., Mainprice, D., 1993. A quantitative evaluation of the contribution of crustal rocks to the shear wave splitting of teleseismic SKS waves. Physics of the Earth and Planetary Interiors 78, 281–300.

Barruol, G., Helffrich, G., Russo, R., Vauchez, A., 1997a. Shear wave splitting around the northern Atlantic: frozen Pangean lithospheric anisotropy? Tectonophysics 279, 135–148.

Barruol, G., Silver, P.G., Vauchez, A., 1997b. Seismic anisotropy in the eastern United States: deep structure of a complex continental plate. Journal of Geophysical Research 102, 8329–8348.

Bastow, I.D., Owens, T.J., Helffrich, G., Knapp, J.H., 2007. Spatial and temporal constraints on sources of seismic anisotropy: evidence from the Scottish Highlands. Geophysical Research Letters 34, L05305, http://dx.doi.org/10.1029/2006gl028911.

Basu, A.R., 1977. Textures, microstructures and deformation of ultramafic xenoliths from San Quintin, Baja California. Tectonophysics 43, 213–245.

Ben Ismaïl, W., Mainprice, D., 1998. An olivine fabric database: an overview of upper mantle fabrics and seismic anisotropy. Tectonophysics 296, 145–158.

Biryol, C.B., Zandt, G., Beck, S.L., Ozacar, A.A., Adiyaman, H.E., Gans, C.R., 2010. Shear wave splitting along a nascent plate boundary: the North Anatolian Fault Zone. Geophysical Journal International 181, 1201–1213.

Bonnin, M., Barruol, G., Bokelmann, G.H.R., 2010. Upper mantle deformation beneath the North American–Pacific plate boundary in California from SKS splitting. Journal of Geophysical Research 115, B04306.

Bostock, M.G., 1997. Anisotropic upper-mantle stratigraphy and architecture of the Slave craton. Nature 390, 392–395.

Bostock, M.G., 1998. Mantle stratigraphy and evolution of the Slave Province. Journal of Geophysical Research 103, 21183–21200.

Bostock, M.G., 1999. Seismic imaging of lithospheric discontinuities and continental evolution. Lithos 48, 1–16.

Boudier, F., 1978. Structure and petrology of the Lanzo massif (Piedmont Alps). Geological Society of America Bulletin 89, 1574–1591.

Boudier, F., Coleman, R.G., 1981. Cross section through the peridotite in the Samail Ophiolite, Southeastern Oman Mountains. Journal of Geophysical Research 86, 2573–2592.

Boudier, F., Ceuleneer, G., Nicolas, A., 1988. Shear zones, thrusts and related magmatism in the Oman ophiolite: initiation of thrusting on an oceanic ridge. Tectonophysics 151, 275–296.

Boullier, A.M., Nicolas, A., 1975. Classification of textures and fabrics of peridotites xenoliths from South African kimberlites. Physics and Chemistry of the Earth 9, 467–475.

Boyd, F.R., 1973. A pyroxene geotherm. Geochimica et Cosmochimica Acta 37, 2533–2538.

Brewer, J.A., Matthews, D.H., Warner, M.R., Hall, J., Smythe, D.K., Whittington, R.J., 1983. BIRPS deep seismic reflection studies of the British Caledonides. Nature 305, 206–210.

Bruijn, R.H.C., Kunze, K., Mainprice, D., Burlini, L., 2011. Mechanical and microstructural development of Carrara marble with pre-existing strain variation. Tectonophysics 503, 75–91.

Butler, R.W.H., Bond, C.E., Shipton, Z.K., Jones, R.R., Casey, M., 2008. Fabric anisotropy controls faulting in the continental crust. Journal of the Geological Society 165, 449–452.

Bystricky, M., Kunze, K., Burlini, L., Burg, J.-P., 2000. High shear strain of olivine aggregates: rheological and seismic consequences. Science 290, 1564–1567.

Cabanes, N., Briqueu, L., 1987. Hydration of an active shear zone: interaction between deformation, metasomatism and metamorphism — the spinel-lherzolites from the Montferrier (Southern France) Oligocene basalts. Earth and Planetary Science Letters 81, 233–244.

Cabanes, N., Mercier, J.C., 1988. Insight into the upper mantle beneath an active extensional zone: the spinel–peridotite xenoliths from San Quintin (Baja California, Mexico). Contributions to Mineralogy and Petrology 100, 374–382.

Caby, R., Andreopoulos-Renaud, U., 1987. Le Hoggar oriental, bloc cratonisé à 730 Ma dans la chaine pan-africaine du nord du continent africain. Precambrian Research 36, 335–344.

Chen, L., Zheng, T., Xu, W., 2006. A thinned lithospheric image of the Tanlu Fault Zone, eastern China: constructed from wave equation based receiver function migration. Journal of Geophysical Research 111, B09312, http://dx.doi.org/10.1029/2005jb003974.

Chevrot, S., 2006. Finite-frequency vectorial tomography: a new method for high-resolution imaging of upper mantle anisotropy. Geophysical Journal International 165, 641–657.

Chopra, P.N., Paterson, M.S., 1981. The experimental deformation of dunite. Tectonophysics 78, 453–473.

Chopra, P.N., Paterson, M.S., 1984. The role of water in the deformation of dunite. Journal of Geophysical Research 86, 7861–7876.

Christensen, N.I., 1971. Fabric, seismic anisotropy and tectonic history of the twin sister dunite, Washington. Geological Society of America Bulletin 82, 1681–1694.

Cook, F.A., van der Velden, A.J., Hall, K.W., Roberts, B.J., 1999. Frozen subduction in Canada's Northwest Territories: lithoprobe deep lithospheric reflection profiling of the western Canadian Shield. Tectonics 18, 1–24.

Copley, A., Hollingsworth, J., Bergman, E., 2012. Constraints on fault and lithosphere rheology from the coseismic slip and postseismic afterslip of the 2006 Mw7.0 Mozambique earthquake. Journal of Geophysical Research 117, B03404.

Crampin, S., 1984. Effective anisotropic elastic constants for wave propagation through cracked solids. Geophysical Journal of the Royal Astronomical Society 76, 135–145.
d'Alessio, M.A., Johanson, I.A., Bürgmann, R., Schmidt, D.A., Murray, M.H., 2005. Slicing up the San Francisco Bay Area: block kinematics and fault slip rates from GPS-derived surface velocities. Journal of Geophysical Research 110, B06403, http://dx.doi.org/10.1029/2004JB003496.
Debayle, E., Kennett, B., Priestley, K., 2005. Global azimuthal seismic anisotropy and the unique plate-motion deformation of Australia. Nature 433, 509–512.
Delle Piane, C., Burlini, L., 2008. Influence of strain history on the mechanical and micro-fabric evolution of calcite rocks: insights from torsion experiments. Swiss Journal of Geosciences 101, 361–375.
Demouchy, S., Jacobsen, S.D., Gaillard, F., Stern, C.R., 2006. Rapid magma ascent recorded by water diffusion profiles in olivine from Earth's mantle. Geology 34, 429–432.
Demouchy, S., Schneider, S.E., Mackwell, S.J., Zimmerman, M.E., Kohlstedt, D.L., 2009. Experimental deformation of olivine single crystals at lithospheric temperatures. Geophysical Research Letters 36, L04304, http://dx.doi.org/10.1029/2008gl036611.
Demouchy, S., Mainprice, D., Tommasi, A., Couvy, H., Barou, F., Frost, D.J., Cordier, P., 2011. Forsterite to wadsleyite phase transformation under shear stress and consequences for the Earth's mantle transition zone. Physics of the Earth and Planetary Interiors 184, 91–104.
Diaconescu, C., Knapp, J., Brown, L., Steer, D., Stiller, M., 1998. Precambrian Moho offset and tectonic stability of the East European Platform from the URSEIS deep seismic profile. Geology 26, 211–214.
Dijkstra, A.H., Drury, M.R., Frijhoff, R.M., 2002a. Microstructures and lattice fabrics in the Hilti mantle section (Oman Ophiolite): evidence for shear localization and melt weakening in the crust–mantle transition zone? Journal of Geophysical Research 107, 2270, http://dx.doi.org/10.1029/2001jb000458.
Dijkstra, A.H., Drury, M.R., Vissers, R.L.M., Newman, J., 2002b. On the role of melt–rock reaction in mantle shear zone formation in the Othris Peridotite Massif (Greece). Journal of Structural Geology 24, 1431–1450.
Dijkstra, A.H., Drury, M.R., Vissers, R.L.M., Newman, J., Van Roermund, H.L.M., 2004. Shear zones in the upper mantle: evidence from alpine- and ophiolite-type peridotite massifs. Geological Society of London, Special Publications 224, 11–24.
Doukhan, N., Doukhan, J.C., FitzGerald, J.D., Chopra, P.N., Paterson, M.S., 1984. A TEM microstructural study of experimentally deformed Anita Bay dunite. In: Tressler, R.E., Bradt, R.C. (Eds.), Deformation of Ceramics II. Plenum Publishing Co., New York, pp. 307–319.
Duclos, M., Savage, M.K., Tommasi, A., Gledhill, K.R., 2005. Mantle tectonics beneath New Zealand inferred from SKS splitting and petrophysics. Geophysical Journal International 163, 760–774.
Durham, W.B., Goetze, G., 1977. Plastic flow of oriented single crystals of olivine. 1. Mechanical data. Journal of Geophysical Research 82, 5737–5753.
Durham, W.B., Goetze, G., Blake, B., 1977. Plastic flow of oriented single crystals of olivine. 2. Observations and interpretations of the dislocation structures. Journal of Geophysical Research 82, 5755–5770.
Ellis, S., Stockhert, B., 2004. Elevated stresses and creep rates beneath the brittle–ductile transition caused by seismic faulting in the upper crust. Journal of Geophysical Research 109, B05407, http://dx.doi.org/10.1029/2003jb002744.
Evans, B., Goetze, C., 1979. The temperature variation of hardness of olivine and its implication for polycrystalline yield stress. Journal of Geophysical Research 84, 5505–5524.
Falus, G., Tommasi, A., Ingrin, J., Szabo, C., 2008. Deformation and seismic anisotropy of the lithospheric mantle in the southeastern Carpathians inferred from the study of mantle xenoliths. Earth and Planetary Science Letters 272, 50–64.
Falus, G., Tommasi, A., Soustelle, V., 2011. Effect of dynamic recrystallization on olivine crystal preferred orientations in mantle xenoliths deformed under varied stress conditions. Journal of Structural Geology 33, 1528–1540.
Fleitout, L., Froidevaux, C., 1980. Thermal and mechanical evolution of shear zones. Journal of Structural Geology 2, 159–164.
Freed, A.M., Herring, T., Burgmann, R., 2010. Steady-state laboratory flow laws alone fail to explain postseismic observations. Earth and Planetary Science Letters 300, 1–10.
Freed, A.M., Hirth, G., Behn, M.D., 2012. Using short-term postseismic displacements to infer the ambient deformation conditions of the upper mantle. Journal of Geophysical Research 117, B01409.
Frets, E.C., Tommasi, A., Garrido, C.J., Padrón-Navarta, J.A., Amri, I., Targuisti, K., 2012. Deformation processes and rheology of pyroxenites deformed under lithospheric mantle conditions. Journal of Structural Geology, http://dx.doi.org/10.1016/j.jsg.2012.02.019.
Furusho, M., Kanagawa, K., 1999. Transformation induced strain localization in a lherzolite mylonite from the Hidaka metamorphic belt of central Hokkaido, Japan. Tectonophysics 313, 411–432.
Garrido, C.J., Gueydan, F., Booth-Rea, G., Précigout, J., Hidas, K., Padron-Navarta, J.A., Marchesi, C., 2011. Garnet lherzolite and garnet–spinel mylonite in the Ronda peridotite: vestiges of Oligocene backarc mantle lithospheric extension in the western Mediterranean. Geology 39, 927–930.
Goscombe, B.D., Gray, D.R., 2008. Structure and strain variation at mid-crustal levels in a transpressional orogen: a review of Kaoko Belt structure and the character of West Gondwana amalgamation and dispersal. Gondwana Research 13, 45–85.
Gourmelen, N., Amelung, F., 2005. Postseismic mantle relaxation in the Central Nevada Seismic Belt. Science 310, 1473–1476.
Growdon, M.A., Pavlis, G.L., Niu, F., Vernon, F.L., Rendon, H., 2009. Constraints on mantle flow at the Caribbean–South American plate boundary inferred from shear wave splitting. Journal of Geophysical Research 114, B02303, http://dx.doi.org/10.1029/2008jb005887.
Gueguen, Y., Nicolas, A., 1980. Deformation of mantle rocks. Annual Review of Earth and Planetary Sciences 8, 119–144.
Guilbert, J., Poupinet, G., Mei, J., 1996. A study of azimuthal P residuals and shear-wave splitting across the Kunlun range (Northern Tibetan plateau). Physics of the Earth and Planetary Interiors 95, 167–174.
Handy, M.R., 1989. Deformation regimes and the rheological evolution of fault zones in the lithosphere: the effects of pressure, temperature, grainsize and time. Tectonophysics 163, 119–152.
Handy, M.R., Hirth, G., Bürgmann, R., 2007. Continental fault structure and rheology from the frictional-to-viscous transition downward. In: Handy, M.R., Hirth, G., Hovius, N. (Eds.), Dahlem Workshop Reports. The MIT Press, Cambridge, USA, pp. 139–181.
Hansen, L.N., Dillman, A.M., Zimmerman, M.E., Kohlstedt, D.L., 2012. Strain localization in olivine aggregates at high temperature: An experimental comparison of constant-strain-rate and constant-stress boundary conditions. Earth and Planetary Science Letters 333–334, 134–145.
Hartog, R., Schwartz, S.Y., 2001. Depth-dependent mantle anisotropy below the San Andreas Fault system: apparent splitting parameters and waveforms. Geophysical Research Letters 106, 4155–4167.
Hearn, T.M., 1996. Anisotropic Pn tomography in the western United States. Journal of Geophysical Research 101, 8403–8414.
Heintz, M., Vauchez, A., Assumpção, M., Barruol, G., Egydio-Silva, M., 2003. Shear wave splitting in SE Brazil: an effect of active or frozen upper mantle flow, or both? Earth and Planetary Science Letters 211, 79–95.
Helffrich, G., 1995. Lithospheric deformation inferred from teleseismic shear wave splitting observations in the United Kingdom. Journal of Geophysical Research 100, 18195–18204.
Herquel, G., Wittlinger, G., 1994. Anisotropy at the Lacq hydrocarbon field (France) from shear-wave splitting. Geophysical Research Letters 21, 2621–2624.
Herquel, G., Tapponnier, P., Wittlinger, G., Mei, J., Danian, S., 1999. Teleseismic shear wave splitting and lithospheric anisotropy beneath and across the Altyn Tagh Fault. Geophysical Research Letters 26, 3225–3228.
Hess, H.H., 1964. Seismic anisotropy of the uppermost mantle under oceans. Nature 203, 629–631.
Hirth, G., Kohlstedt, D., 2003. Rheology of the upper mantle and the mantle wedge: A view from the experimentalists. In: Eiler, J. (Ed.), Inside the subduction factory. : Geophysical monograph, 138. American Geophysical Union, pp. 83–105.
Holdsworth, R.E., Stewart, M., Imber, J., Strachan, R.A., 2001. The structure and rheological evolution of reactivated continental fault zones: a review and case study. Geological Society of London, Special Publications 18, 115–137.
Hollenstein, C., Mḷler, M.D., Geiger, A., Kahle, H.G., 2008. Crustal motion and deformation in Greece from a decade of GPS measurements, 1993–2003. Tectonophysics 449, 17–40.
Holtzman, B.K., Groebner, N.J., Zimmerman, M.E., Ginsberg, S.B., Kohlstedt, D.L., 2003. Stress-driven melt segregation in partially molten rocks. Geochemistry, Geophysics, Geosystems 4, 8607.
Holyoke III, C.W., Tullis, J., 2006. Formation and maintenance of shear zones. Geology 34, 105–108.
Hoogerduijn Strating, E.H., Rampone, E., Piccardo, G.B., Drury, M.R., Vissers, R.L.M., 1993. Subsolidus emplacement of mantle peridotites during incipient oceanic rifting and opening of the Mesozoic Tethys (Voltri Massif, NW Italy). Journal of Petrology 34, 901–927.
Jaroslow, G.E., Hirth, G., Dick, H.J.B., 1996. Abyssal peridotite mylonites: implications for grain-size sensitive flow and strain localization in the oceanic lithosphere. Tectonophysics 256, 17–37.
Ji, S., Rondenay, S., Mareschal, M., Senechal, G., 1996. Obliquity between seismic and electrical anisotropies as a potential indicator of movement sense for ductile shear zones in the upper mantle. Geology 24, 1033–1036.
Jones, A.G., Kurtz, R.D., Boerner, D.E., Craven, J.A., McNeice, G.W., Gough, D.I., DeLaurier, J.M., Ellis, R.G., 1992. Electromagnetic constraints on strike-slip fault geometry—the Fraser River fault system. Geology 20, 561–564.
Judenherc, S., Granet, M., Boumbar, N., 1999. Two-dimensional anisotropic tomography of lithosphere beneath France using regional arrival times. Journal of Geophysical Research 104, 13201–13215.
Jung, H., Katayama, I., Jiang, Z., Hiraga, T., Karato, S., 2006. Effect of water and stress on the lattice-preferred orientation of olivine. Tectonophysics 421, 1–22.
Kaczmarek, M.-A., Tommasi, A., 2011. Anatomy of an extensional shear zone in the mantle (Lanzo massif, Italy). Geochemistry, Geophysics, Geosystems Q0AG06, http://dx.doi.org/10.1029/2011GC003627.
Kaviani, A., Hatzfeld, D., Paul, A., Tatar, M., Priestley, K., 2009. Shear-wave splitting, lithospheric anisotropy, and mantle deformation beneath the Arabia–Eurasia collision zone in Iran. Earth and Planetary Science Letters 286, 371–378.
Kelemen, P.B., Dick, H.J.B., 1995. Focused melt flow and localized deformation in the upper mantle: juxtaposition of replacive dunite and ductile shear zones in the Josephine peridotite, SW Oregon. Journal of Geophysical Research 100, 423–438.
Keller, L.M., Götze, L.C., Rybacki, E., Dresen, G., Abart, R., 2010. Enhancement of solid-state reaction rates by non-hydrostatic stress effects on polycrystalline diffusion kinetics. American Mineralogist 95, 1399–1407.
Khazaradze, G., Wang, K., Klotz, J., Hu, Y., He, J., 2002. Prolonged post-seismic deformation of the 1960 great Chile earthquake and implications for mantle rheology. Geophysical Research Letters 29, 2050, http://dx.doi.org/10.1029/2002gl015986.
Kind, R., Yuan, X., Saul, J., Nelson, D., Sobolev, S.V., Mechie, J., Zhao, W., Kosarev, G., Ni, J., Achauer, U., Jiang, M., 2002. Seismic images of crust and upper mantle beneath Tibet: evidence for Eurasian plate subduction. Science 298, 1219–1221.
King, D.S.H., Zimmerman, M.E., Kohlstedt, D.L., 2010. Stress-driven melt segregation in partially molten olivine-rich rocks deformed in torsion. Journal of Petrology 51, 21–42.
Klosko, E.R., Wu, F.T., Anderson, H.J., Eberhart Phillips, D., McEvilly, T.V., Audoine, E., Savage, M.K., Gledhill, K.R., 1999. Upper mantle anisotropy in the New Zealand region. Geophysical Research Letters 26, 1497–1500.

Knoll, M., Tommasi, A., Logé, R.E., Signorelli, J.W., 2009. A multiscale approach to model the anisotropic deformation of lithospheric plates. Geochemistry, Geophysics, Geosystems 10, Q08009, http://dx.doi.org/10.1029/2009gc002423.
Le Roux, V., Tommasi, A., Vauchez, A., 2008. Feedback processes between percolation and deformation in a frozen lithosphere–asthenosphere boundary. Earth and Planetary Science Letters 274, 401–413.
Leloup, P.H., Lacassin, R., Tapponnier, P., Schärer, U., Dalai, Z., Xiaohan, L., Liangshang, Z., Shaocheng, J., Trinh, P.T., 1995. The Ailao Shan–Red River shear zone (Yunnan, China), Tertiary transform boundary of Indochina. Tectonophysics 251, 3–84.
Levin, V., Park, J., 2000. Shear zones in the Proterozoic lithosphere of the Arabian Shield and the nature of the Hales discontinuity. Tectonophysics 323, 131–148.
Li, Y., Wu, Q., Zhang, F., Feng, Q., Zhang, R., 2011. Seismic anisotropy of the Northeastern Tibetan Plateau from shear wave splitting analysis. Earth and Planetary Science Letters 304, 147–157.
Lin, F.-C., Ritzwoller, M.H., Snieder, R., 2009. Eikonal tomography: surface wave tomography by phase front tracking across a regional broad-band seismic array. Geophysical Journal International 177, 1091–1110.
Lindenfeld, M., Rümpker, G., 2011. Detection of mantle earthquakes beneath the East African Rift. Geophysical Journal International 186, 1–5.
Lu, G., Kaus, B.J.P., Zhao, L., 2011. Thermal localization as a potential mechanism to rift cratons. Physics of the Earth and Planetary Interiors 186, 125–137.
Mainprice, D., Silver, P.G., 1993. Interpretation of SKS-waves using samples from the subcontinental lithosphere. Physics of the Earth and Planetary Interiors 78, 257–280.
Mainprice, D., Barruol, G., Ben Ismaïl, W., 2000. The seismic anisotropy of the Earth's mantle: from single crystal to polycrystal. In: Karato, S.-I., Forte, A.M., Liebermann, R.C., Masters, G., Stixrude, L. (Eds.), Earth's deep interior: mineral physics and seismic tomography: from atomic to global: AGU Geophysics Monograph, pp. 237–264.
Mareschal, M., Kellet, R.L., Kurtz, R.D., Ludden, J.N., Ji, S., Bailey, R.C., 1995. Archean cratonic roots, mantle shear zones and deep electrical anisotropy. Nature 375, 134–137.
Marson-Pidgeon, M., Savage, M.K., Gledhill, K., Stuart, G., 1999. Seismic anisotropy beneath the lower half of the North Island, New Zealand. Journal of Geophysical Research 104, 20277–20286.
Martelat, J.-E., Schulmann, K., Lardeaux, J.-M., Nicollet, C., Cardon, H., 1999. Granulite microfabrics and deformation mechanisms in southern Madagascar. Journal of Structural Geology 21, 671–687.
McBride, J.H., Snyder, D.B., Tate, M.P., England, R.W., Hobbs, R.W., 1995. Upper mantle reflector structure and origin beneath the Scottish Caledonides. Tectonics 14, 1351–1367.
McClusky, S., Balassanian, S., Barka, A., Demir, C., Ergintav, S., Georgiev, I., Gurkan, O., Hamburger, M., Hurst, K., Kahle, H., Kastens, K., Kekelidze, G., King, R., Kotzev, V., Lenk, O., Mahmoud, S., Mishin, A., Nadariya, M., Ouzounis, A., Paradissis, D., Peter, Y., Prilepin, M., Reilinger, R., Sanli, I., Seeger, H., Tealeb, A., Toksˆz, M.N., Veis, G., 2000. Global Positioning System constraints on plate kinematics and dynamics in the eastern Mediterranean and Caucasus. Journal of Geophysical Research 105, 5695–5719.
McGeary, S., Warner, M.R., 1985. Seismic profiling the continental lithosphere. Nature 317, 795–797.
McNamara, D., Owens, T.J., Silver, P.G., Wu, F.T., 1994. Shear wave anisotropy beneath the Tibetan Plateau. Journal of Geophysical Research 99, 13655–13665.
Mercier, J.-C., Nicolas, A., 1975. Textures and fabrics of upper mantle peridotites as illustrated by xenoliths from basalts. Journal of Petrology 16, 454–487.
Meshi, A., Boudier, F., Nicolas, A., Milushi, I., 2010. Structure and tectonics of lower crustal and upper mantle rocks in the Jurassic Mirdita ophiolites, Albania. International Geology Review 52, 117–141.
Michibayashi, K., Mainprice, D., 2004. The role of pre-existing mechanical anisotropy on shear zone development within oceanic mantle lithosphere: an example from the Oman ophiolite. Journal of Petrology 45, 405–414.
Michibayashi, K., Ohara, Y., Stern, R.J., Fryer, P., Kimura, J.I., Tasaka, M., Harigane, Y., Ishii, T., 2009. Peridotites from a ductile shear zone within back-arc lithospheric mantle, southern Mariana Trench: results of a Shinkai 6500 dive. Geochemistry, Geophysics, Geosystems 10, Q05X06, http://dx.doi.org/10.1029/2008GC002197.
Miller, M.S., Eaton, D.W., 2010. Formation of cratonic mantle keels by arc accretion: evidence from S receiver functions. Geophysical Research Letters 37, L18305, http://dx.doi.org/10.1029/2010GL044366.
Mjelde, R., Sellevoll, M.A., 1993. Seismic anisotropy inferred from wide-angle reflections off Lofoten, Norway, indicative of shear-aligned minerals in the upper mantle. Tectonophysics 222, 21–32.
Monsalve, G., McGovern, P., Sheehan, A., 2009. Mantle fault zones beneath the Himalayan collision: flexure of the continental lithosphere. Tectonophysics 477, 66–76.
Montagner, J.P., Kennett, B.L.N., 1996. How to reconcile body-wave and normal-mode reference earth models. Geophysical Journal International 125, 229–248.
Montesi, L.G.J., 2004. Controls of shear zone rheology and tectonic loading on postseismic creep. Journal of Geophysical Research 109, B10404, http://dx.doi.org/10.1029/2001jb000465.
Montési, L.G.J., Zuber, M.T., 2002. A unified description of localization for application to large-scale tectonics. Journal of Geophysical Research 107, 2045, http://dx.doi.org/10.1029/2001jb000465.
Neves, S.P., Tommasi, A., Vauchez, A., 2008. Intraplate continental deformation: influence of a heat-producing layer in the lithospheric mantle. Earth and Planetary Science Letters 274, 392–400.
Newman, J., Drury, M.R., 2010. Control of shear zone location and thickness by initial grain size variations in upper mantle peridotites. Journal of Structural Geology 32, 832–842.
Newman, J., Lamb, W.M., Drury, M.R., Vissers, R.L.M., 1999. Deformation processes in a peridotite shear zone: reaction-softening by an H_2O-deficient, continuous net transfer reaction. Tectonophysics 303, 193–222.
Nicolas, A., Boudier, F., 2008. Large shear zones with no relative displacement. Terra Nova 20, 200–205.
Nicolas, A., Christensen, N.I., 1987. Formation of anisotropy in upper mantle peridotites — a review. In: Fuchs, K., Froidevaux, C. (Eds.), Composition, Structure and Dynamics of the Lithosphere–Asthenosphere System. American Geophysical Union, Washington, D.C., pp. 111–123.
Nicolas, A., Bouchez, J.L., Boudier, F., Mercier, J.C., 1971. Textures, structures and fabrics due to solid state flow in some European lherzolites. Tectonophysics 12, 55–86.
Nicolas, A., Bouchez, J.L., Boudier, F., 1972. Interprétation cinématique des déformations plastiques dans le massif de lherzolites de Lanzo. Tectonophysics 14, 143–171.
Nicolas, A., Boudier, F., Boullier, A.M., 1973. Mechanism of flow in naturally and experimentally deformed peridotites. American Journal of Science 273, 853–876.
Nicolas, A., Boudier, F., Bouchez, J.L., 1980. Interpretation of peridotite structures from ophiolitic and oceanic environments. American Journal of Science 280, 192–210.
Obata, M., 1980. The Ronda peridotite: garnet-, spinel-, and plagioclase-lherzolite facies and the P–T trajectories of a high-temperature mantle intrusion. Journal of Petrology 21, 533–572.
Ozalaybey, S., Savage, M.K., 1994. Double-layer anisotropy resolved from S phases. Geophysical Journal International 117, 653–664.
Ozalaybey, S., Savage, M.K., 1995. Shear wave splitting beneath the western United States in relation to plate tectonics. Journal of Geophysical Research 100, 18135–18149.
Paterson, M.S., 2007. Localization in rate-dependent shearing deformation, with application to torsion testing. Tectonophysics 445, 273–280.
Peslier, A.H., 2010. A review of water contents of nominally anhydrous natural minerals in the mantles of Earth, Mars and the Moon. Journal of Volcanology and Geothermal Research 197, 239–258.
Phakey, P., Dollinger, G., Christie, J., 1972. Transmission electron microscopy of experimentally deformed olivine crystals. In: Heard, H.C., Borg, I.Y., Carter, N.L., Rayleigh, C.B. (Eds.), Flow and Fracture of Rocks. American Geophysical Union, Washington, DC, pp. 117–138.
Pieri, M., Burlini, L., Kunze, K., Stretton, I., Olgaard, D.L., 2001a. Rheological and microstructural evolution of Carrara marble with high shear strain: results from high temperature torsion experiments. Journal of Structural Geology 23, 1393–1413.
Pieri, M., Kunze, K., Burlini, L., Stretton, I., Olgaard, D.L., Burg, J.P., Wenk, H.R., 2001b. Texture development of calcite by deformation and dynamic recrystallization at 1000 K during torsion experiments of marble to large strains. Tectonophysics 330, 119–140.
Pili, Kennedy, B.M., Conrad, M.E., Gratier, J.P., 2011. Isotopic evidence for the infiltration of mantle and metamorphic CO_2–H_2O fluids from below in faulted rocks from the San Andreas Fault system. Chemical Geology 281, 242–252.
Platt, J.P., Behr, W.M., 2011. Lithospheric shear zones as constant stress experiments. Geology 39, 127–130.
Poe, B.T., Romano, C., Nestola, F., Smyth, J.R., 2010. Electrical conductivity anisotropy of dry and hydrous olivine at 8 GPa. Physics of the Earth and Planetary Interiors 181, 103–111.
Pollitz, F.F., 2005. Transient rheology of the upper mantle beneath central Alaska inferred from the crustal velocity field following the 2002 Denali earthquake. Journal of Geophysical Research 110, B08407, http://dx.doi.org/10.1029/2005JB003672.
Pollitz, F.F., Thatcher, W., 2010. On the resolution of shallow mantle viscosity structure using postearthquake relaxation data: application to the 1999 Hector Mine, California, earthquake. Journal of Geophysical Research 115, B10412, http://dx.doi.org/10.1029/2010JB007405.
Pollitz, F.F., Peltzer, G., Bürgmann, R., 2000. Mobility of continental mantle: evidence from postseismic geodetic observations following the 1992 Landers earthquake. Journal of Geophysical Research 105, 8035–8054, http://dx.doi.org/10.1029/1999JB900380.
Pollitz, F.F., Wicks, C., Thatcher, W., 2001. Mantle Flow beneath a continental strike-slip fault: postseismic deformation after the 1999 Hector Mine earthquake. Science 293, 1814–1818.
Regenauer-Lieb, K., Yuen, D., 2004. Positive feedback of interacting ductile faults from coupling of equation of state, rheology and thermal-mechanics. Physics of the Earth and Planetary Interiors 142, 113–135.
Reilinger, R., McClusky, S., Vernant, P., Lawrence, S., Ergintav, S., Cakmak, R., Ozener, H., Kadirov, F., Guliev, I., Stepanyan, R., Nadariya, M., Hahubia, G., Mahmoud, S., Sakr, K., ArRajehi, A., Paradissis, D., Al-Aydrus, A., Prilepin, M., Guseva, T., Evren, E., Dmitrotsa, A., Filikov, S.V., Gomez, F., Al-Ghazzi, R., Karam, G., 2006. GPS constraints on continental deformation in the Africa–Arabia–Eurasia continental collision zone and implications for the dynamics of plate interactions. Journal of Geophysical Research 111, B05411, http://dx.doi.org/10.1029/2005JB004051.
Reston, T.J., 1990. Shear in the lower crust during extension: not so pure and simple. Tectonophysics 173, 175–183.
Reuber, I., 1984. Mylonitic ductile shear zones within tectonites and cumulates as evidence for an oceanic transform fault in the Antalya ophiolite, S.W. Turkey. Geological Society of London, Special Publications 17, 319–334.
Reuber, I., Michard, A., Chalouan, A., Juteau, T., Jermoumi, B., 1982. Structure and emplacement of the Alpine-type peridotites from Beni Bousera, Rif, Morocco: a polyphase tectonic interpretation. Tectonophysics 82, 231–251.
Ross, J.V., 1977. The internal fabric of an alpine peridotite near Pinchi Lake, central British Columbia. Canadian Journal of Earth Sciences 14, 32–44.
Ross, J.V., Mercier, J.-C.C., Xu, Y., 1996. Diffusion creep in the upper mantle: an example from the Tanlu Fault, northeastern China. Tectonophysics 261, 315–329.
Rümpker, G., Ryberg, T., Bock, G., Desert Seismology Group, 2003. Boundary-layer mantle flow under the Dead Sea transform fault inferred from seismic anisotropy. Nature 425, 497–501.
Rümpker, G., Silver, P.G., 1998. Apparent shear-wave splitting parameters in the presence of vertically varying anisotropy. Geophysical Journal International 135, 790–800.
Russo, R.M., Silver, P.G., Franke, M., Ambeh, W.B., James, D.E., 1996. Shear wave splitting in northeast Venezuela, Trinidad, and the eastern Caribbean. Physics of the Earth and Planetary Interiors 95, 251–275.

Rutter, E.H., 1998. Use of extension testing to investigate the influence of finite strain on the theological behaviour of marble. Journal of Structural Geology 20, 243–254.
Rutter, E.H., 1999. On the relationship between the formation of shear zones and the form of the flow law for rocks undergoing dynamic recrystallization. Tectonophysics 303, 147–158.
Rutter, E.H., Brodie, K.H., 1988. The role of grain size reduction in the rheological stratification of the lithosphere. Geologische Rundschau 77, 295–308.
Rybacki, E., Paterson, M.S., Wirth, R., Dresen, G., 2003. Rheology of calcite–quartz aggregates deformed to large strain in torsion. Journal of Geophysical Research 108, 2089.
Rychert, C.A., Shearer, P.M., 2009. A global view of the lithosphere–asthenosphere boundary. Science 324, 495–498.
Salvini, F., Brancolini, G., Busetti, M., Storti, F., Mazzarini, F., Coren, F., 1997. Cenozoic geodynamics of the Ross Sea region, Antarctica: crustal extension, intraplate strike-slip faulting, and tectonic inheritance. Journal of Geophysical Research 102, 24669–24696.
Sandvol, E., Turkelli, N., Zor, E., Gok, R., Bekler, T., Gurbuz, C., Seber, D., Barazangi, M., 2003. Shear wave splitting in a young continent–continent collision: an example from Eastern Turkey. Geophysical Research Letters 30, 8041, http://dx.doi.org/10.1029/2003GL017390.
Savage, M.K., 1999. Seismic anisotropy and mantle deformation: what have we learned from shear wave splitting? Reviews of Geophysics 37, 65–106.
Sawaguchi, T., 2004. Deformation history and exhumation process of the Horoman Peridotite Complex, Hokkaido, Japan. Tectonophysics 379, 109–126.
Sénéchal, G., Rondenay, S., Mareschal, M., Guilbert, J., Poupinet, G., 1996. Seismic and electrical anisotropies in the lithosphere across the Grenville Front, Canada. Geophysical Research Letters 23, 2255–2258.
Şengör, A.M.C., Tüysüz, O., İmren, C., Sakınç, M., Eyidoğan, H., Görür, N., Le Pichon, X., Rangin, C., 2005. The North Anatolian Fault: a new look. Annual Review of Earth and Planetary Sciences 33, 37–112.
Shi, D., Zhao, W., Brown, L., Nelson, D., Zhao, X., Kind, R., Ni, J., Xiong, J., Mechie, J., Guo, J., Klemperer, S., Hearn, T., 2004. Detection of southward intracontinental subduction of Tibetan lithosphere along the Bangong–Nujiang suture by P-to-S converted waves. Geology 32, 209–212.
Sibson, R.H., 1977. Fault rocks and fault mechanisms. Journal of the Geological Society of London 133, 191–213.
Silver, P.G., Chan, W.W., 1991. Shear wave splitting and subcontinental mantle deformation. Journal of Geophysical Research 96, 16429–16454.
Silver, P.G., Savage, M.K., 1994. The interpretation of shear wave splitting parameters in the presence of two anisotropic layers. Geophysical Journal International 119, 949–963.
Silver, P.G., Mainprice, D., Ben Ismail, W., Tommasi, A., Barruol, G., 1999. Mantle structural geology from seismic anisotropy. In: Fei, Y., Bertka, C.M., Mysen, B.O. (Eds.), Mantle Petrology: Field Observations and High Pressure Experimentation: A Tribute to Francis R. (Joe) Boyd. The Geochemical Society, Washington, pp. 79–103.
Skemer, P., Warren, J.M., Kelemen, P.B., Hirth, G., 2010. Microstructural and rheological evolution of a mantle shear zone. Journal of Petrology 51, 43–53.
Smythe, D.K., Dobinson, A., McQuillin, R., Brewer, J.A., Matthews, D.H., Blundell, D.J., Kelk, B., 1982. Deep structure of the Scottish Caledonides revealed by the MOIST reflection profile. Nature 299, 338–340.
Snyder, D.B., 2008. Stacked uppermost mantle layers within the Slave craton of NW Canada as defined by anisotropic seismic discontinuities. Tectonics 27, TC4006.
Soustelle, V., Tommasi, A., Bodinier, J.L., Garrido, C.J., Vauchez, A., 2009. Deformation and reactive melt transport in the mantle lithosphere above a large-scale partial melting domain: the Ronda Peridotite Massif, Southern Spain. Journal of Petrology 50, 1235–1266.
Storti, F., Holdsworth, R.E., Salvini, F., 2003. Intraplate strike-slip deformation belts. In: Storti, F., Holdsworth, R.E., Salvini, F. (Eds.), Intraplate strike-slip deformation belts: Geological Society of London, Special Publication, 210, pp. 1–14.
Suhr, G., 1993. Evaluation of upper mantle microstructures in the Table Mountain massif (Bay of Islands ophiolite). Journal of Structural Geology 15, 1273–1292.
Sykes, L.R., 1978. Intraplate seismicity, reactivation of preexisting zones of weakness, alkaline magmatism, and other tectonism postdating continental fragmentation. Reviews of Geophysics and Space Physics 13, 621–688.
ten Grotenhuis, S.M., Drury, M.R., Peach, C.J., Spiers, C.J., 2004. Electrical properties of fine-grained olivine: evidence for grain boundary transport. Journal of Geophysical Research 109, B06203, http://dx.doi.org/10.1029/2003jb002799.
Teyssier, C., Tikoff, B., 1998. Strike-slip partitioned transpression of the San Andreas Fault system: a lithospheric approach. In: Holdsworth, R.A., Strachan, R.A., Dewey, J.F. (Eds.), Continental transpressional and transtensional deformation: Geological Society of London, Special Publication, pp. 143–158.
Thatcher, W., 2007. Microplate model for the present-day deformation of Tibet. Journal of Geophysical Research 112, B01401, http://dx.doi.org/10.1029/2005jb004244.
Tilley, C.E., 1947. The dunite–mylonites of Saint Paul's Rocks (Atlantic). American Journal of Science 245, 483–491.
Titus, S.J., Medaris, L.G., Wang, H.F., Tikoff, B., 2007. Continuation of the San Andreas Fault system into the upper mantle: evidence from spinel peridotite xenoliths in the Coyote Lake basalt, central California. Tectonophysics 429, 1–20.
Tommasi, A., Vauchez, A., 2001. Continental rifting parallel to ancient collisional belts: an effect of the mechanical anisotropy of the lithospheric mantle. Earth and Planetary Science Letters 185, 199–210.
Tommasi, A., Vauchez, A., Daudré, B., 1995. Initiation and propagation of shear zones in a heterogeneous continental lithosphere. Journal of Geophysical Research 100, 22083–22101.
Tommasi, A., Tikoff, B., Vauchez, A., 1999. Upper mantle tectonics: three-dimensional deformation, olivine crystallographic fabrics and seismic properties. Earth and Planetary Science Letters 168, 173–186.
Tommasi, A., Mainprice, D., Canova, G., Chastel, Y., 2000. Viscoplastic self-consistent and equilibrium-based modeling of olivine lattice preferred orientations. 1. Implications for upper mantle seismic anisotropy. Journal of Geophysical Research 105, 7893–7908.
Tommasi, A., Gibert, B., Seipold, U., Mainprice, D., 2001. Anisotropy of thermal diffusivity in the upper mantle. Nature 411, 783–786.
Tommasi, A., Vauchez, A., Godard, M., Belley, F., 2006. Deformation and melt transport in a highly depleted peridotite massif from the Canadian Cordillera: implications to seismic anisotropy above subduction zones. Earth and Planetary Science Letters 252, 245–259.
Tommasi, A., Knoll, M., Vauchez, A., Signorelli, J., Logé, R., 2009. Structural reactivation in plate tectonics controlled by olivine crystal anisotropy. Nature Geoscience 2, 423–427.
Tubia, J.M., Cuevas, J., 1987. Structures et cinématique liées à la mise en place des peridotites de Ronda (Cordilleres Betiques, Espagne). Geodinamica Acta 1, 59–69.
Van der Wal, D., Vissers, R.L.M., 1996. Structural petrology of the Ronda peridotite, SW Spain: deformation history. Journal of Petrology 37, 23–43.
Vauchez, A., Garrido, C.J., 2001. Seismic properties of an asthenospherized lithospheric mantle: constraints from lattice preferred orientations in peridotite from the Ronda Massif. Earth and Planetary Science Letters 192, 235–249.
Vauchez, A., Nicolas, A., 1991. Mountain building: strike-parallel displacements and mantle anisotropy. Tectonophysics 185, 183–201.
Vauchez, A., Tommasi, A., 2003. Wrench faults down to the asthenosphere: geological and geophysical evidence and thermo-mechanical effects. In: Storti, F., Holdsworth, R.E., Salvini, F. (Eds.), Intraplate strike-slip deformation belts. Special Publication, 210. Geological Society of London, pp. 15–34.
Vauchez, A., Barruol, G., Tommasi, A., 1997. Why do continents break up parallel to ancient orogenic belts? Terra Nova 9, 62–66.
Vauchez, A., Tommasi, A., Barruol, G., 1998. Rheological heterogeneity, mechanical anisotropy, and tectonics of the continental lithosphere. Tectonophysics 296, 61–86.
Vauchez, A., Dineur, F., Rudnick, R.L., 2005. Microstructure, texture and seismic anisotropy of the lithospheric mantle above a mantle plume. Insights from the Labait volcano xenoliths (Tanzania). Earth and Planetary Science Letters 232, 295–314.
Vauchez, A., Egydio-Silva, M., Babinski, M., Tommasi, A., Uhlein, A., Liu, D., 2007. Deformation of a pervasively molten middle-crust: insights from the neoproterozoic Ribeira–Araçuaí orogen (SE Brazil). Terra Nova 19, 278–286.
Vergnolle, M., Pollitz, F., Calais, E., 2003. Constraints on the viscosity of the continental crust and mantle from GPS measurements and postseismic deformation models in western Mongolia. Journal of Geophysical Research 108, 2502–2514.
Vernant, P., Nilforoushan, F., Hatzfeld, D., Abassi, M.R., Vigny, C., Masson, F., Nankali, H., Martinod, J., Ashtiani, M., Bayer, R., Tavakoli, F., Chéry, J., 2004. Present-day crustal deformation and plate kinematics in the Middle East constrained by GPS measurements in Iran and northern Oman. Geophysical Journal International 157, 381–398.
Vilotte, J.-P., Madariaga, R., Daignières, M., Zienkiewicz, O., 1984. The role of a heterogeneous inclusion during continental collision. Physics of the Earth and Planetary Interiors 36, 236–259.
Vinnik, L.P., Makeyeva, L.I., Milev, A., Usenko, A.Y., 1992. Global patterns of azimuthal anisotropy and deformations in the continental mantle. Geophysical Journal International 111, 433–437.
Vissers, R.L.M., Drury, M.R., Strating, E.H.H., Van der Wal, D., 1991. Shear zones in the upper mantle: a case study in an Alpine Iherzolite massif. Geology 19, 990–993.
Vissers, R.L.M., Drury, M.R., Hoogerduijn Strating, E.H., Spiers, C.J., van der Wal, D., 1995. Mantle shear zones and their effect on lithosphere strength during continental breakup. Tectonophysics 249, 155–171.
Vissers, R.L.M., Drury, M.R., Newman, J., Vlirvoert, T.F., 1997. Mylonitic deformation in upper mantle peridotites of the North Pyrenean Zone (France): implications for strength and strain localization in the lithosphere. Tectonophysics 279, 303–325.
Warren, J.M., Hirth, G., 2006. Grain size sensitive deformation mechanisms in naturally deformed peridotites. Earth and Planetary Science Letters 248, 438–450.
Warren, J.M., Hirth, G., Kelemen, P.B., 2008. Evolution of olivine lattice preferred orientation during simple shear in the mantle. Earth and Planetary Science Letters 272, 501–512.
Webber, C., Newman, J., Holyoke Iii, C.W., Little, T., Tikoff, B., 2010. Fabric development in cm-scale shear zones in ultramafic rocks, Red Hills, New Zealand. Tectonophysics 489, 55–75.
Wenk, H.-R., Bennet, K., Canova, G.R., Molinari, A., 1991. Modelling plastic deformation of peridotite with the self-consistent theory. Journal of Geophysical Research 96, 8337–8349.
Wilson, J.T., 1966. Did the Atlantic close and then re-open? Nature 211, 676–681.
Wilson, R.W., Holdsworth, R.E., Wild, L.E., McCaffrey, K.J.W., England, R.W., Imber, J., Strachan, R.A., 2010. Basement-influenced rifting and basin development: a reappraisal of post-Caledonian faulting patterns from the North Coast Transfer Zone, Scotland. Geological Society of London, Special Publications 335, 795–826.
Wittlinger, G., Tapponnier, P., Poupinet, G., Mei, J., Danian, S., Herquel, G., Masson, F., 1998. Tomographic evidence for localized lithospheric shear along the Altyn Tagh Fault. Science 282, 74–76.
Yuan, H., Romanowicz, B., 2010. Lithospheric layering in the North American craton. Nature 466, 1063–1068.
Zhang, P.-Z., Shen, Z., Wang, M., Gan, W., Burgmann, R., Molnar, P., Wang, Q., Niu, Z., Sun, J., Wu, J., Hanrong, S., Xinzhao, Y., 2004. Continuous deformation of the Tibetan Plateau from global positioning system data. Geology 32, 809–812.
Zhang, S., Karato, S.I., 1995. Lattice preferred orientation of olivine aggregates deformed in simple shear. Nature 375, 774–777.
Zerka, M., Cottin, J.-Y., Gregoire, M., Lorand, J.-P., Megartsi, M., Midoun, M., 2002. Ultramafic xenoliths from Quaternary alkali volcanism from Oranie (Tell, western

Algeria): witnesses of a sheared and enriched lithosphere. Comptes Rendus de l'Academie des Sciences - Series IIA - Earth and Planetary Science 334, 387–394.
Zhao, Y.-H., Ginsberg, S.B., Kohlstedt, D.L., 2004. Solubility of hydrogen in olivine: dependence on temperature and iron content. Contributions to Mineralogy and Petrology 147, 155–161.
Zimmerman, M.E., Kohlstedt, D.L., 2004. Rheological Properties of Partially Molten Lherzolite. Journal of Petrology 45, 275–298.
Zimmerman, M.E., Zhang, S., Kohlstedt, D.L., Karato, S., 1999. Melt distribution in mantle rocks deformed in shear. Geophysical Research Letters 26, 1505–1508.